Optimal charging and state-of-charge estimation of a Lithium-ion cell using a simplified full homogenised macro-scale model

Salman Qadir

Submitted in partial fulfilment of the requirements
of the Degree of Doctor of Philosophy

School of Engineering and Material Sciences

Queen Mary University of London

United Kingdom

June 2022

Statement of originality

I, Salman Qadir, confirm that the research included within this thesis is my own work or that where it has been carried out in collaboration with, or supported by others, that this is duly acknowledged below and my contribution indicated. Previously published material is also acknowledged below.

I attest that I have exercised reasonable care to ensure that the work is original, and does not to the best of my knowledge break any UK law, infringe any third party's copyright or other Intellectual Property Right, or contain any confidential material.

I accept that the Queen Mary University of London has the right to use plagiarism detection software to check the electronic version of the thesis.

I confirm that this thesis has not been previously submitted for the award of a degree by this or any other university.

Signature: Salman Qadir

Date: 13-06-2021

List of publications

- Qadir, Salman, Guang Li, and Zheng Chen. "Simplification of full homogenized macro-scale model for lithium-ion batteries." Journal of Energy Storage 46 (2022).
- Qadir, Salman, and Guang Li. "Health-Conscious Optimal Control of Li-ion Cell using Simplified Full Homogenised Macro-scale Model." (under review).
- Qadir, Salman, and Guang Li. "Output Feedback Health-Conscious Control of Li-ion Cell using Simplified Full Homogenised Macro-scale Model." (In preparation).

Abstract

Advanced battery management systems (BMS) need accurate and computationally efficient Li-ion cell model for optimum operation as the performance of charging and estimation algorithms of BMS are dependent upon the accuracy of the mathematical model of a cell. This research work presents a novel, accurate and computationally efficient electrochemical model and develops charging and estimation algorithm based on the model. The simplified model is based on the novel full homogenised macro-scale model (FHM). The simplified FHM model is compared with a simplified model based on the pseudo-two-dimensional (P2D) model. The FHM model is based on the homogenisation theory, while the volume averaging technique is the basis of the P2D model. Diffusion partial differential equations (PDEs) are approximated by ordinary differential equations with time-varying coefficients. The intercalation current and conduction equation are also approximated to develop variants of the simplified model. The diffusion and reaction rate parameters of the FHM model are more accurate at high temperatures than the parameters based on the empirical Bruggeman method, as the FHM model parameters are based on the numerical model of the electrode structure. The simulations results verify that, compared with a similar simplified model based on the P2D model, the proposed simplified FHM model is more accurate at 318K and higher temperature. The output voltage predicted by the proposed simplified model and the simplified P2D model has a root mean square (RMS) tracking error of 0.6% and 2%, respectively, at 1C input current and 318K temperature. The computational time of the proposed simplified model is reduced by 35% compared with that of the FHM model. Subsequently we present optimal charging of Li-ion cell based on the simplified full homogenised macro-scale (FHM) model. A solid electrolyte interface (SEI) layer model

is included in the simplified FHM model to quantify health degradation. With these models, a multi-objective optimal control problem subject to constraints from safety concerns is formulated to achieve the health-conscious optimal charging. This constrained optimal control problem is converted to a nonlinear programming problem (NLP). A nonlinear model predictive control (NMPC) strategy is adopted by solving the NLP at each sampling time using the pseudo-spectral optimisation method. The effect of the input current upper bound on the cell film resistance R_{film} and state of health (SoH) reveals that R_{film} and SoH are more sensitive to input current upper bound at lower values of input current upper bound. Simulation results show that the simplified model and pseudo-spectral method are crucial for reducing the computational load to achieve feasible real-time implementation. The proposed algorithm is more efficient in reducing the health degradation than the conventional constant current constant voltage ($CCCV$) charging algorithm since it can explicitly handle the film resistance and capacity as health parameters. Multiple cycle charging simulation reveals that the health-conscious algorithm decrease health degradation and increase battery life.

Three observers are used and compared for output feedback charging of a Li-ion cell, i.e. extended Kalman filter (EKF), sliding mode observer (SMO) and moving horizon estimator (MHE). The observers are used in a closed-loop with an NMPC for optimal, health-conscious charging of a Li-ion cell. Simulation results show that EKF and SMO have a low computational burden, whereas MHE exhibits superior performance.

[He] who created death and life to test you [as to] which of you is best in deeds and He is the exalted in might, the forgiving.

Quran[67:2]

Acknowledgements

All praises are due to Allah for giving me the abilities, resources and courage to pursue a research career.

I am grateful to my family, relatives and friends for the support i received throughout my life.

A heartfelt thanks to Queen Mary university of London and Dr Guang Li for accepting me as a PhD student, and for the thought-provoking discussions we shared. His comments brought this manuscript to a significant improvement.

I feel privileged to have this many eminent researchers in my committee. Thanks for accepting to be part of it.

Contents

List of Figures

List of Tables

Chapter 1

Introduction of thesis

1.1 Motivation of the research

Li-ion battery technology offers high energy density, long cycle life, and low self-discharge rate compared to other battery technologies. Using the cell efficiently and maintaining health is vital for its performance and reducing ageing speed. A battery management system (BMS) manages the operation of cells to achieve these goals.

The fidelity of a battery model is essential for designing an efficient BMS. Equivalent circuit models (ECMs) are the simplest and computationally efficient Li-ion cell models. [12], [13]. However, ECMs are not a desirable choice as they do not provide insight into the electrochemical properties of Li-ion cells. By contrast, electrochemical models provide insight into the physical processes happening in the cell, such as diffusion, conduction, intercalation current, and solid electrolyte interface (SEI) layer growth. However, the complexities of electrochemical models can introduce a heavy computational load for the BMS algorithms designed based on these models.

One way to reduce the computational load of the algorithms based on the electrochemical models is to use a simplified model to approximate its dynamics while not sacrificing too much fidelity. The computational complexity and the fidelity need to be traded off correctly when an electrochemical model is simplified to be suitable for the BMS algorithm design purpose.

Motivated by the fact that efficient BMS needs a model having high fidelity, low com-

putational burden, and provides a better understanding of battery dynamics. We have presented a simplified model based on Full Homogenised Macro-scale (FHM) model. The model is more accurate than state-of-the-art simplified electrochemical models based on the Doyle–Fuller–Newman (DFN) model. We have also presented health-conscious charging and estimation based on this model.

1.2 Aim of the thesis

This thesis focuses on model simplification, health-conscious optimal charging, and estimation of a Li-ion cell based on the full homogenised macro-scale (FHM) model. The literature review reveals that the FHM model is more accurate than state-of-the-art electrochemical models at high temperatures and a low state of charge (SoC). We have shown that the performance of the health-conscious optimal charging and estimation algorithms based on the simplified FHM model will be more reliable and accurate than their state-of-the-art mathematical counterpart. Multiple variants of the simplified model allow users to trade off computational load for accuracy. To reduce the computational burden, we have used pseudo-spectral discretisation.

1.3 Literature review and contribution of the research

1.3.1 Contribution I: Mathematical modelling of a Li-ion cell

A Battery management system (BMS) plays a vital role in ensuring the battery's safe operation in various conditions to optimise the battery efficiency. BMS monitors essential state variables of the cell, such as state of charge (SoC), state of health (SoH), and temperature, among others, to avoid misuse of the battery [14] [5].

The mathematical model of a Li-ion cell is an essential part of BMS to estimate the state variables. Over the past decades, numerous mathematical models have been developed with a range of computational complexity and accuracy, such as equivalent circuit models, data-driven models, and electrochemical models [8], [15], [16].

Equivalent circuit models are simple and computationally efficient as compared to other models. Equivalent circuit models are composed of electric circuit elements such as voltage sources, resistors, and capacitors, as shown in figure 1.1. These fictitious elements are added to obtain a current-voltage characteristic curve equivalent to a Li-ion cell's experimental current-voltage characteristic curve. The battery states such as SoC and SoH calculated using the equivalent circuit models are less accurate than the computationally intensive electrochemical models [12], [13]. Consider figure 1.1, Open circuit voltage OCV is obtained empirically. OCV is a function of the cell's state of charge SoC. A fully charged cell is discharged for a small-time duration. After discharging, the cell is kept at rest for a specific time, and open circuit voltage is measured. The process is repeated until the cell is completely discharged. The SoC and OCV data points are used to make an empirical function of OCV in terms of SoC using nonlinear regression. R_0 models the internal resistance of the Li-ion cell. The RC circuit is included to model the effect of diffusion of a Li-ion cell. As the diffusion of Li-ion cell is a slow process, it is modelled by a first-order low pass filter using RC circuit. System identification algorithms such as particle swarm optimisation are applied to experimental data sets of a Li-ion cell to estimate other parameters of an equivalent circuit model. Equivalent circuit models are also used to estimate a Li-ion cell's state of health SoH. By calculating the change in internal resistance R_0 and the Li-ion cell's capacity, the cell's SoH can be calculated. A cell's health degrades if its internal resistance rises and capacity declines. The equivalent circuit model shown in figure 1.1 is a simple variant. Its accuracy can be enhanced by adding more RC pairs and other elements to include the effects, such as hysteresis. The application of equivalent circuit models to the battery management system is extensively studied. Meng *et al.*, Zhang *et al.* and Xiasong *et al.* have compared various variants of equivalent circuit models of Li-ion cell [17], [18],[19]. The equivalent circuit model variants are thoroughly reviewed in these articles. In addition to the benefits and drawbacks of various equivalent circuit model variations, authors have also discussed parameter estimation techniques, model validation, SoC and SoH estimation.

Recently attempts have been made to improve SoC estimation using either advanced

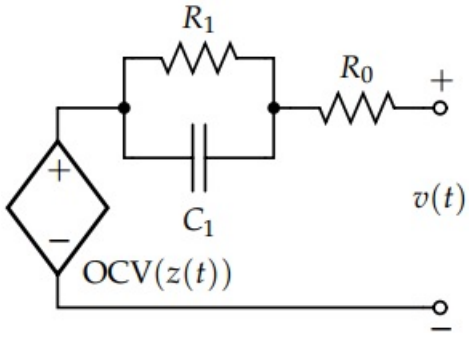

Figure 1.1: Equivalent circuit model of a Li-ion cell [1].

equivalent circuit models or adaptive neuro-fuzzy inference systems (ANFIS) based models. However, the proposed models need to be more accurate or health-conscious enough as compared to electrochemical models [20], [21], [22], [23]. L. Ma *et al.* has proposed joint *SoC* estimation based on a long short-term memory neural network. The approach shows better results compared to other machine learning algorithms, but it is not accurate enough compared to the proposed approach [24]. H Yang *et al.* and H F Khan *et al.* have proposed *SoC* estimation based on variants of the Kalman filter. However, the model used is a basic equivalent circuit model. The performance can be improved further by using accurate models [25], [26].

Electrochemical models are derived from the first principles of the cell, such as the Doyle Fuller Newman (DFN) model [27]. Electrochemical models precisely describe the internal dynamics of the cell, such as diffusion, conduction, and intercalation. The DFN model consists of five equations. Two equations describe the diffusion process in electrode and electrolyte, whereas two equations describe the conduction process in electrode and electrolyte. The exchange of Li-ion between the electrode and electrolyte is described by the intercalation current equation, which combines the four equations. These equations are derived from the fundamentals of a cell, which are based on the atomic-scale physical processes occurring in cells. Electrochemical models are more reliable than equivalent circuit models due to their high accuracy. Second, compared to the internal resistance of an equivalent circuit model of a Li-ion cell, the parameters of the electrochemical model—such as diffusion parameter, conduction parameter, and film resistance are more indicative of the health of the Li-ion cell. However, using an

electrochemical model such as the DFN model for real-time processing is not feasible due to the high computational load. DFN model is mainly used as a reference to evaluate the accuracy of other simplified models.

A reduced electrochemical model is imperative for real-time processing [28], [29]. Numerous approaches have been used to simplify the DFN model. The single-particle model is a popularly used simplified electrochemical model. The model is named the single particle model because the electrode diffusion is described using a spherical particle model. The intercalation current equation is considered to be constant. By making this assumption, the other four equations of the DFN model are decoupled, and the algebraic loop is removed, reducing the computational load of the model and greatly simplifying the numerical integration. Some works proposed a constant Li-ion concentration in the electrolyte to further simplify the model. Electrolyte equations are disregarded in this approximation. The temperature dependence of the parameters has been taken into account in some studies to improve the model accuracy. [30], [31], [32]. Another method for developing a reduced model of a Li-ion cell is to approximate spatial double derivatives in diffusion equations of electrode and electrolyte with time-varying polynomials, as done by Subramanian [33], Han *et al.* [10] and Deng *et al.*, [2]. A thermal model of a Li-ion cell based on the first principle is also studied. The physics-based thermal models have higher accuracy than those developed for equivalent circuit models. A range of thermal models are available for full electrochemical models and reduced electrochemical models to trade-off computational complexity and accuracy [34], [35], [36].

The models mentioned above are nonlinear. Linear electrochemical models are created using Taylor series expansion as proposed by Smith *et al.* [37] and Le *et al.* [38]. The linear equations are then converted to transfer functions using Laplace theory. The proposed method, however, yields complicated transcendental transfer functions. Ngoc *et al.* solved this problem by converting transcendental transfer functions into simpler rational polynomial transfer functions using pade approximation[39]. It has been observed that pade approximation decreases algorithm execution time by around 50 times. The earlier-mentioned efforts are based on classical system theory. Lee *et al.* has proposed a discrete-time realisation algorithm (DRA) to develop a physics-based linear state space

model for a Li-ion cell [40]. The author uses a sample-and-hold framework along with an inverse discrete Fourier transform to generate a discrete impulse response in this method. Ho Kalman filter is then used to transform discrete impulse response into a state space matrix.

Diffusion and conduction parameters of the DFN model are key parameters that influence the fidelity of the DFN model. The empirical Bruggeman method is used to obtain the parameters for the DFN model. The method leads to inaccurate results in certain conditions [7]. Recently a more accurate model called the full homogenised macro-scale (FHM) model has been developed. The FHM model is developed using homogeneity theory, whereas the DFN model uses volume averaging. FHM model inculcates the structural composition of the electrode and calculates the value of diffusion and conduction parameters D_e, D_s, K_e and K_s by developing a numerical model of electrode architecture. The model is more accurate for estimation in conditions such as low values of SoC, a high value of temperature and a C-rate. However, the performance of both models is similar at room temperature [6], [41]. The FHM model is computationally intensive and suitable for offline estimation and analysis.

A one-dimensional FHM and DFN model is considered in this research work. A 'pseudo' spherical dimension r is included in the DFN model to describe the diffusion of Li-ions within electrode particles. The model is also known as the pseudo-two-dimensional (P2D) Model [42].

The P2D model fails to accurately predict the cell's output voltage at high temperatures, i.e. above $318K$ and low value of charge [6]. The performance of P2D-based simplified models deteriorates further at a high input current value due to approximation.

Novelty

We present a simplified model based on the FHM model, which is computationally less intensive than the FHM model but more accurate than the simplified P2D model at high temperatures. We expect the simplified FHM model to show performance similar

to the FHM model up to a $4C$ input current, which enables us to develop an accurate model fast enough to be implementable in real time.

The idea of the proposed model is similar to the simplified models developed by Subramanian *et al.* [33], Han *et al.* [10] and Deng *et al.* [2]. The articles, as mentioned earlier, are based on the idea that ordinary differential equations with time-varying coefficients can approximate the Li-ion concentration. Replacement of the spatial double derivative with time-varying coefficients simplifies the models and facilitates fast implementation. We have used a second-order polynomial to approximate the Li-ion concentration in electrodes and electrolyte. High-order polynomials can be used for approximation for increasing accuracy, as suggested by Subramanian [33]. However, Ricardo *et al.* has suggested that high-order polynomials also create undesirable features such as higher transient errors. [43].

1.3.2 Contribution II: Optimal charging of a Li-ion cell

A charging strategy is important to charge a Li-ion cell in minimum time without damaging the battery and extending the life of a Li-ion cell. Numerous strategies for efficient battery charging have been developed, including simple charging, optimised charging, model-based charging, and AC charging. [44], [45], [46], [33]. Zhang investigated the effect of various charging protocols on the cycle life of a Li-ion cell [47]. Constant current constant voltage ($CCCV$) is the most widely used optimal charging algorithm for Li-ion cells. The battery is initially charged using a constant input current in this charging method. In this charging mode, known as constant current (CC), the input current is normally set to its maximum value. In CC charging mode, the Li-ion cell voltage gradually increases until it reaches a maximum value. When the SoC reaches 100 %, the cell enters constant voltage (CV) charging mode, in which the cell is charged at a constant voltage and the input current steadily approaches zero. Another method of charging is the multi-step constant current (MCC) method. This charging method includes several modes. The cell is charged with a different constant input current value during each mode. MCC charges faster and more efficiently and leads to less temperature

rise as compared to *CCCV* charging [48], [49]. There are better algorithms than the *CCCV* and MCC algorithms to optimise the health of Li-ion cells as they are not based on the battery model. Researchers have proposed many model-free charging protocols, such as pulse charging protocol, boost charging protocol, variable duty voltage pulse charging, variable frequency pulse charging and variable current profile; each method has its pros and cons. All model free charging algorithms have one drawback, i.e., they are not health conscious [50], [51].

Model-based charging algorithms are better candidates for minimising health loss because they are better aware of cell dynamics and charging regimes that harm the cell. The simplest model of Li-ion cells is an equivalent circuit model. Researchers attempted to develop a charging algorithm based on equivalent circuit models and an optimising algorithm to minimise Li-ion cell health degradation. Many health-conscious optimal controllers have been suggested using either equivalent circuit models or simplified electrochemical models recently [52],[53]. For example, Xiaosong *et al.* has proposed an optimal multistage charging algorithm using an equivalent circuit model to reduce cell ageing. The algorithm performs better than the *CCCV* charging algorithm; however, capacity fade is the only parameter used as a figure of merit for comparison [54]. Perez *et al.* has proposed health-conscious optimal charging based on an equivalent circuit model. The health of a Li-ion cell is monitored by developing a coupled electrothermal battery ageing model [55]. However, equivalent circuit models are effective at simulating the input-output behaviour of lithium-ion cells. Internal cell dynamics related to Li-ion cell health are not adequately described by equivalent circuit models such as solid electrolyte interphase (SEI) layer growth, Li-ion deposition, and mechanical degradation of a cell. [51]. Many researchers present modelling of the health-related parameters of battery [56], [57], [58], and [59]. Yang *et al.* and Khalik *et al.* have proposed a health-conscious charging algorithm based on a single particle model [60], [54]. Pozzi *et al.* has proposed an optimal charging algorithm based on a P2D model to increase the cycle life of a Li-ion cell [61]. Hu *et al.* has proposed health conscious charging algorithm based on a single particle model to minimise Li-ion plating [62]. The algorithms mentioned above are health-conscious and based on an electrochemical model, making them a better

candidate for charging than the $CCCV$ charging and equivalent circuit model-based health-conscious controllers. However, we expect that the performance will degrade at high temperatures due to model inaccuracy, as reported by Arunachalam *et al.* [7], [6].

Novelty

The second novel contribution of this work includes health-conscious optimal control of a Li-ion cell using a simplified FHM model. To make the optimal control health-conscious, the SEI layer model mentioned in [56], [63], and [57] is included in the simplified FHM model. The comparison between the optimal health-conscious charging algorithm and the $CCCV$ algorithm using the simplified FHM model shows that the health-conscious charging algorithm outperforms the optimal $CCCV$ charging algorithm by reducing the degradation in film resistance R_{film} and SoH. The effect of the input current upper bound on the control algorithm is also examined. The study reveals that the health parameters, i.e., R_{film} and SoH, change significantly for low input current upper bound values, i.e., $1C$. The SoH value at the end of a single cycle converges to a constant value for high values of the input current upper bound, and the upper bound becomes ineffective. The performance of algorithms for multiple cycles reveals that the health-conscious algorithm outperforms the $CCCV$ algorithm by increasing the battery's useful life and reducing film resistance. For the numerical implementation of the optimal charging algorithm, orthogonal collocation is used to decrease algorithm execution time.

1.3.3 Contribution III: Output feedback optimal charging of a Li-ion cell

Estimation is imperative for designing model-based charging strategies of Li-ion cells as control law requires complete knowledge of system states. Generally, only input current and output voltage are available signals. States of a cell such as SoC, SoH, electrolyte Li-ion concentration and electrode Li-ion concentration are unknown and need to be

estimated.

Multiple approaches are available to estimate Li-ion cell states. A direct method such as coulomb counting is inaccurate and prone to noise as an error with time. However, the computational load is low. Machine learning methods are relatively less accurate and have a high computation burden. However, machine learning methods work without a mathematical model of the battery. Model-based estimation methods have relatively high accuracy and high computational load. Equivalent circuit models have frequently been used to estimate Li-ion cell dynamics. He *et al.* has presented a detailed review of research contributions about SoC estimations based on equivalent circuit models [64]. SoC estimation based on equivalent circuit models is more accurate than direct methods. However, as discussed earlier equivalent circuit can not describe internal dynamics. Among model-based estimation methods, electrochemical models have the extra benefit of better describing the internal dynamics of the battery as they can describe the physical processes of the battery. Electrochemical models are more accurate as compared to equivalent circuit models. SoC and SoH estimation of a Li-ion cell using electrochemical models are extensively studied.

A mathematical model cannot accurately predict system behaviour if observers or estimators do not minimise the effect of noise and parameter uncertainties. Using adaptive filters and observers increases the accuracy of estimators considerably. However, the price paid is a high computational cost.

Several observers have been used to estimate Li-ion cell states based on electrochemical models, for example, extended Kalman filter, unscented Kalman filter, particle filter, H infinity estimator, back-stepping observer, and recursive least square estimator. The performance comparison of these algorithms is available in literature [65], [16]. Moving horizon estimation has the additional benefit of systematically handling constraints while estimating system states at the cost of additional computation burden. Moving horizon estimation has been extensively used to estimate Li-ion cell dynamics using equivalent circuits and electrochemical models. [66], [67], [68], [69], [70], [71], [72], [73], [74], [75], [76]. Previous research about MHE has yet to explore nonlinear MHE and nonlinear MPC for output feedback charging of a Li-ion cell based on an electrochemical

model. Output feedback means the controller and observer are used in a closed loop. The controller generates the input current based on the estimate of the Li-ion cell's states provided by the observer online. Suthar *et al.* has used nonlinear MHE for state estimation based on a reformulated model. Although nonlinear MPC is also presented, nonlinear MPC and nonlinear MHE are not used in a closed loop for output feedback charging [66].

Novelty

The algorithms used for Li-ion cell SoC estimation are based on state-of-the-art equivalent circuit models and electrochemical models such as the single particle model (SPM) and polynomial approximated P2D model. A simplified FHM model is not used to estimate Li-ion cell dynamics till now. The third novel contribution of this work is the estimation of Li-ion cell states using estimators such as EKF, SMO and MHE for output feedback, health-conscious, pseudo-spectral, and charging of a Li-ion cell based on a simplified FHM model. The performance of the three estimation algorithms is compared in the open loop in the presence of zero-mean additive white Gaussian noise and parameter perturbation in the system. Comparison of closed-loop estimation using MPC yields results similar to the open-loop case. Another novelty of the work is the use of nonlinear MHE and nonlinear MPC for output feedback charging which is not done based on other models. The algorithm execution time per iteration for all algorithms is less than the sampling time, making real-time implementation of the output feedback charging algorithm feasible. Results show the superior performance of MHE as compared to EKF and SMO. However, EKF and SMO are computationally efficient as compared to MHE. The SEI layer model mentioned in [56], [63], and [57] is also included in the simplified FHM model. The robustness of the estimation algorithm is assessed by adding additive white Gaussian noise to the Li-ion cell's output voltage and perturbing parameters of the mathematical model.

1.4 Organisation of the dissertation

The research work can be divided into modelling, charging and estimation. Each part is discussed in a separate chapter. The details of the chapters are given as follows.

In Chapter 2, We discuss the mathematical modelling of a Li-ion cell. All mathematical models used in the research work are discussed. We explain the state-of-the-art electrochemical model, such as a P2D model. Subsequently, we discuss an FHM model and make a comparison with the P2D model. The simplified model based on the P2D model is discussed next. Then simplified model based on the FHM model is proposed. The performance of the proposed model is compared to the SPM using simulations. Temporal discretisation, spatial discretisation and the pseudo-spectral method are also discussed in chapter 2.

Health-conscious optimal charging of a Li-ion cell based on a simplified FHM model is discussed in chapter 3. The solid electrolyte inter-phase (SEI) layer model for the simplified FHM model is discussed. Next, the optimal control problem (OCP) is presented based on the simplified FHM and coupled SEI layer models. The OCP is converted to a nonlinear programming problem (NLP) using a pseudo-spectral method. The NLP is solved using a nonlinear model predictive controller. The performance of the health-conscious controller is compared with the industry standard $CCCV$ charging algorithm under various conditions.

Output feedback charging is discussed in chapter 4. Observers such as extended Kalman filter (EKF), sliding mode observer (SMO) and moving horizon estimator (MHE) are used to predict Li-ion cell states. A pseudo-spectral method is used to develop NLP for the moving horizon estimation method. Simulation results using the three estimators are compared and analysed under various conditions, such as the presence of additive white Gaussian noise and parameter perturbation. In the end, we compare the simulation results of the closed-loop control problem when MPC is included in the loop for output feedback charging.

Conclusions and future work suggestions are discussed in Chapter 5.

Chapter 2

Mathematical modelling of a Li-ion cell

2.1 Introduction of mathematical modelling

A mathematical system model describes a system's working under various scenarios. For safe, optimal and efficient use of a battery, we need the knowledge of system states and constraints. We also need the knowledge of the conditions or scenarios that profoundly affect system health and performance, such as very high or low temperature, heavy load and high speed of an EV. A mathematical model is developed to achieve these objectives. For example, a battery's state of charge (SoC) provides information about the charge stored in the battery as a percentage of total charge and can be considered the 'fuel gauge' of an EV. SoC of a cell and all other states, such as cell output voltage and cell health, can be computed using the mathematical model of a cell.

An essential feature of a mathematical model is computational complexity. A highly accurate model is only feasible for real-time implementation if the computing resources are sufficient to simulate the model in real time. Finding the right balance between accuracy and computational complexity is essential to developing an accurate model which can be implemented in computing systems in real-time.

As discussed earlier, electrochemical models have a distinguishing feature of accurately describing the internal dynamics of a Li-ion cell as they are derived from the first

principles of a Li-ion cell. Other mathematical models can only describe the output and input relationship and do not provide meaningful insight into the internal dynamics of a Li-ion cell. Equivalent circuit models are the simplest and computationally most efficient but not as accurate as electrochemical models. Data-driven models are computationally intensive, but mathematical modelling of the cell is not required. A detailed comparison of the modelling techniques is available in literature [77],[17],[78],[79].

Electrochemical models such as the Doyle Fuller Newman (DFN) and FHM are known for high accuracy. These models describe the cell's internal dynamics, such as diffusion, conduction, and intercalation. Electrochemical models are more reliable than equivalent circuit models due to their high accuracy. However, due to the high computational load, A reduced electrochemical model is imperative for real-time processing. A schematic of a Li-ion cell is shown in figure 2.1 for illustration purposes.

Numerous reduced models have been developed to trade off models' computational load and accuracy. The Full-order electrochemical models consist of five equations (two PDEs and three algebraic equations). Each equation represents a physical phenomenon in the battery during the charging or discharging operation. The two PDEs describe the diffusion happening in electrodes and electrolyte, whereas the two algebraic equations describe conduction in electrodes and electrolyte. The third algebraic equation, i.e. Butler Volmer equation, combines the effect of four equations and describes the exchange of Li-ions (known as intercalation and de-intercalation) between electrodes and electrolyte. The model reduction attempts for the full-order model comprise simplifying these five equations.

The most important simplification step is to simplify the Butler-Volmer equation to decouple the other four equations of a Li-ion cell. The simplification is accomplished by assuming the intercalation current as constant. This simplification leads to a simplified model known as the single particle model [30], [80]. Other attempts include approximating electrode diffusion equation PDE with time-varying ODE as done by Subramanian *et al.* [81] or approximating electrolyte diffusion equation PDE with time-varying ODE as done by Han *et al.* and Deng *et al.* [10], [2]. The simplification is achieved by approximating spatial derivatives with time-varying polynomials. Orthogonal collocation on Chebyshev

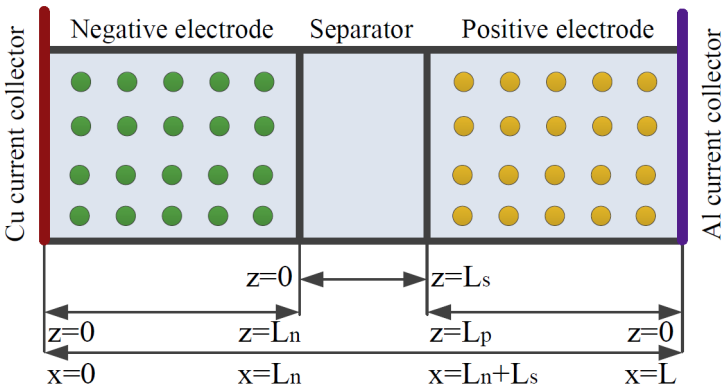

Figure 2.1: Li-ions cell schematic [2].

polynomials is used for the fast numerical implementation of the algorithms without losing accuracy [82],[42].

Although some researchers have recommended high-order polynomials [33], we prefer the second-order polynomial to approximate the Li-ion concentration in electrodes and electrolyte. Recently it has been observed that the approximate electrode models developed using higher-order polynomials introduce unwanted characteristics, such as eigenvalues with positive real parts, and non-minimum phase zeros. In contrast, the actual electrode model does not exhibit these characteristics. However, Second-order polynomials provide smaller bandwidth and less precision in transients compared to higher-order polynomial approximations [43]. Another feature of polynomials is time variance. The coefficients of polynomials are calculated at every iteration.

This chapter will initially present a brief comparison of the FHM and DFN models. We present multiple variants of reduced electrochemical models based on the FHM model. The numerical implementation of the mathematical model is discussed in section 2.4. Discretisation in the time and the spatial domain is discussed in detail in section 2.4. A comparison of the simplified FHM model with the reduced model based on the DFN model is presented in section 2.5.

Eq. No	FHM Model	P2D Model	Part
(2.1)	$\frac{\partial c_{s,j}(z,t)}{\partial t} = D_{s,j}\frac{\partial^2 c_{s,j}(z,t)}{\partial z^2} - \frac{J_j(z,t)}{F}$	$\frac{\partial c_{s,j}(z,r,t)}{\partial t} = \frac{1}{r^2}\frac{\partial}{\partial r}\Big(D_{s,j}r^2\frac{\partial c_{s,j}(z,r,t)}{\partial r}\Big)$	Electrode Diffusion
(2.2)	$\eta_{e,j}\frac{\partial c_{e,j}(z,t)}{\partial t} = \frac{J_j(z,t)}{F} + D_{e,j}\frac{\partial^2 c_{e,j}}{\partial z^2}$ $+\frac{RTt_+^2}{F^2}K_{e,j}\frac{\partial^2 ln\ c_{e,j}}{\partial z^2} + \frac{t_+}{F}K_{e,j}\frac{\partial^2\phi_{e,j}}{\partial z^2}$	$\eta_{e,j}\frac{\partial c_{e,j}(z,t)}{\partial t} = \frac{\partial}{\partial z}\Big(D_{e,j}\frac{\partial c_{e,j}}{\partial z}\Big)$ $+\frac{(1-t_+)J_j(z,t)}{F}$	Electrolyte Diffusion
(2.3)	$K_{s,j}\frac{\partial^2\phi_{s,j}(z,t)}{\partial z^2} = J_j(z,t)$	$K_{s,j}\frac{\partial^2\phi_{s,j}(z,t)}{\partial z^2} = J_j(z,t)$	Electrode Potential
(2.4)	$\frac{RTt_+}{F}K_{e,j}\frac{\partial^2 lnc_{e,j}}{\partial z^2} + K_{e,j}\frac{\partial^2\phi_{e,j}(z,t)}{\partial z^2}$ $= -J_j(z,t)$	$\frac{2RT(1-t_+)}{F}K_{e,j}\frac{\partial^2 lnc_{e,j}}{\partial z^2} + K_{e,j}\frac{\partial^2\phi_{e,j}(z,t)}{\partial z^2}$ $= -J_j(z,t)$	Electrolyte Potential
(2.5)	$\eta_j = \phi_{s,j}(z) - \phi_{e,j}(z) - U_{c,j}(\theta)$ $i_{0,j} = ((c_{e,j}c_{s,j})(1-\frac{c_{s,j}}{c_{j,m}}))^{0.5}$ $J_j(z,t) = i_{0,j}2k_j sinh\Big(\frac{F\eta_j}{2RT}\Big)$	$\eta_j = \phi_{s,j}(z) - \phi_{e,j}(z) - U_{c,j}(\theta)$ $i_{0,j} = ((c_{e,j}c_{s,j})(c_{j,m}-c_{s,j}))^{0.5}$ $J_j(z,t) = i_{0,j}2k_j\ \cdot sinh\Big(\frac{F\eta_j}{2RT}\Big)$	Intercalation Current

Table 2.1: Comparison of P2D and FHM mathematical models [7]

2.2 Full order electrochemical models of a Li-ion cell

2.2.1 Pseudo two dimensional (P2D) model

The cell's electrodes are assumed to be made up of multiple spherical particles. The diffusion equation describes the P2D electrode diffusion dynamics for a single particle (2.1). The variable r defines the radial dimension of a single particle. $D_{s,j}$ is the diffusion constant that determines the rate of diffusion of Li-ions in an electrode. The diffusion parameter is a temperature dependent parameter. The temperature dependence of diffusion parameter is shown in the figures 2.4 and 2.6. The value of other parameters of the model is given in tables 2.3 and 2.4. The exchange of Li-ions between electrodes and electrolyte, known as intercalation current, occurs at the particle's surface. The boundary conditions at the centre and surface of spherical particles are mentioned as follows.

$$\frac{\partial c_{s,j}}{\partial r}\Big|_{r=0} = 0, \quad \frac{\partial c_{s,j}}{\partial r}\Big|_{r=R_s} = -\frac{J_j}{F\cdot a_j} = \frac{-J_j\cdot R_{s,j}}{D_{s,j}\cdot F\cdot 3\eta_j} \tag{2.6}$$

The boundary condition at the centre of the particle implies that net Li-ion diffusion at the centre is zero as the total no of Li-ion from left to right equals no of Li-ions moving from right to left. This assumption holds for all directions as charged can not be stored at a single point. The Li-ion diffusion at the surface is equivalent to the intercalation current scaled by Faraday's constant F and the electrode interfacial surface area a_s to

account for the porosity of the electrode. Intercalation current is, by definition, equal to the exchange of Li-ions between electrode and electrolyte. As the particle surface is the only area where the exchange occurs, the intercalation current variable is only mentioned in the particle surface boundary condition, unlike the other boundary condition and the diffusion equation. $R_{s,j}$ and $c_{s,j}$ are the radius of the spherical particle and solid concentration, respectively. Initial concentration is given by the initial stoichiometry variable $\theta_{j,init}$, i.e. the normalised value of concentration. Subscript $j = s, n, p$ is used for the separator, anode and cathode, respectively.

The equation (2.2) describes the Li-ion diffusion inside the electrolyte. Initial, boundary and continuity conditions are mentioned in the equations (2.10) and (2.13), respectively. $c_{e,j}$, T and z are the liquid phase (electrolyte) concentration, cell temperature and physical dimension variable, respectively. The electrode of a cell is immersed in an electrolyte, due to which the movement of Li-ion in the liquid phase is affected. Electrolyte volume fraction $\eta_{e,j}$ is included to account for the tortuosity of electrolyte. t_+ is the transference number and is the ratio of cat ions or positive ions current to the total current when there is no potential gradient in the electrolyte. The transference number is responsible for reducing concentration polarisation in electrolyte. L, L_n, L_s and L_p are the length of the cell, anode, separator and cathode, respectively. The rate of Li-ion diffusion in the electrolyte is directly proportional to the electrolyte diffusion parameter D_e. The initial value of the electrolyte concentration is constant and mentioned in table 2.4. The electrolyte boundary condition implies no Li-ion flow between the electrolyte and the current collector. The electrolyte medium exists in a continuum throughout the cell. The continuity conditions of electrolyte indicate that the concentration and the Li-ion flux are equal at both sides of the electrode-separator interface.

Equation (2.5) describes the intercalation current J_j, which by definition is equal to the Li-ion exchange between electrodes and electrolyte. Intercalation depends on all the state and algebraic variables of a Li-ion cell, i.e. Li-ion concentration in electrode and electrolyte, potential in electrode and electrolyte and open circuit potential. The magnitude of intercalation current is directly proportional to reaction rate parameter k_j. Reaction rate parameter is temperature dependent parameter as shown in the figures

2.5 and 2.7. The open circuit potential of a cell is the potential of individual electrodes when the cell is at rest for a certain time and not connected to a circuit. The open circuit potential is given as follows.

$$U_{c,p}(\theta) = -10.72\theta^4 + 23.88\theta^3 - 16.77\theta^2 + 2.595\theta + 4.563 \tag{2.7}$$

$$\begin{aligned} U_{c,n}(\theta) = 0.1493 + 0.8493\exp(-61.79\theta) + 0.3824\exp(-665.8\theta) - 1\exp(39.42\theta - 41.92) \\ -0.03131\arctan(25.59\theta - 4.099) - 0.009434\arctan(32.49\theta - 15.74) \end{aligned} \tag{2.8}$$

η_j is the over-potential and denotes the potential difference between electrode and electrolyte required for the Li-ion exchange between electrode and electrolyte. $\phi_{s,j}$ and $\phi_{e,j}$ are the electrode potential and electrolyte potential respectively. Open circuit potential expressions are empirical, i.e. derived from experiments. We have obtained the expressions as mentioned above from Tanim's work [34]. θ_j, $c_{j,m}$, k_j, T and R are the normalised solid concentration, maximum solid concentration, reaction rate parameter, temperature, and the universal gas constant, respectively.

The dynamics of the solid phase potential drop $\phi_{s,j}$ and liquid phase potential drop $\phi_{e,j}$ is given by the equations (2.4) and (2.3) respectively. $K_{s,j}$ and $K_{e,j}$ are the conductivity parameters for solid and liquid, respectively. Initial conditions and boundary conditions of electrode and electrolyte are described by the equations (2.11) and (2.12), respectively. The equation (2.14) describes the continuity conditions of the electrolyte potential. The initial value of the electrolyte potential drop is assumed zero due to zero electric current in an electrolyte. In contrast, the initial potential drop across the electrode is equal to the open circuit potential as the electrodes store electric charge. The solid potential at the anode collector is considered the reference potential, whereas Ohms's law gives the solid potential at the cathode. The value of the potential drop in the electrolyte at the electrode-collector interface is zero, as the electric charge in the liquid phase, i.e. Li-ions, does not move to the external circuit. The liquid phase potential exists in a continuum throughout the cell, i.e. the liquid phase concentration and flux are equal at both sides of the electrodes-separator inter-phase.

Equation Number	Initial conditions	Boundary conditions	Part
(2.9)	$c_{s,n} = \theta_{n,init} \cdot c_{s,n,m}$ $c_{s,p} = \theta_{p,init} \cdot c_{s,p,m}$	-	Electrode Diffusion
(2.10)	$c_{e,n} = c_{e,sep} = c_{e,p} = c_{e,a}$	$\frac{\partial c_{e,j}}{\partial z}\big\vert_{z=0,L} = 0$	Electrolyte Diffusion
(2.11)	$\phi_{s,n} = 0$ $\phi_{s,p} = U_{p,init} - U_{n,init}$	$\phi_{s,n}\big\vert_{z=0} = 0$ $\frac{\partial \phi_{s,p}}{\partial z}\big\vert_{z=L} = -\frac{I_{app}}{A_{cell} \cdot K_{s,p}}$	Electrode Potential
(2.12)	$\phi_{e,n} = \phi_{e,sep} = \phi_{e,p} = 0$	$\frac{\partial \phi_{e,j}}{\partial x}\Big\vert_{z=0,L} = 0$	Electrolyte Potential
(2.13)	–	$\frac{\partial c_{e,j}}{\partial z}\big\vert_{z=L_{n-}} = \frac{\partial c_{e,j}}{\partial z}\big\vert_{z=L_{n+}}$ $c_{e,j}\big\vert_{x=L_{n-}} = c_{e,j}\big\vert_{z=L_{n+}}$ $\frac{\partial c_{e,j}}{\partial x}\big\vert_{z=L_n+L_{s-}} = \frac{\partial c_{e,j}}{\partial z}\big\vert_{z=L_n+L_{s+}}$ $c_{e,j}\big\vert_{z=L_n+L_{s-}} = c_{e,j}\big\vert_{z=L_n+L_{s+}}$	Electrolyte Diffusion Continuity Equation
(2.14)	–	$\frac{\partial \phi_{e,j}}{\partial z}\big\vert_{z=L_{n-}} = \frac{\partial \phi_{e,j}}{\partial x}\big\vert_{z=L_{n+}}$ $\phi_{e,j}\big\vert_{z=L_{n-}} = \phi_{e,j}\big\vert_{z=L_{n+}}$ $\frac{\partial \phi_{e,j}}{\partial x}\big\vert_{z=L_n+L_{s-}} = \frac{\partial \phi_{e,j}}{\partial z}\big\vert_{z=L_n+L_{s+}}$ $\phi_{e,j}\big\vert_{z=L_n+L_{s-}} = \phi_{e,j}\big\vert_{z=L_n+L_{s+}}$	Electrolyte Potential Continuity Equation

Table 2.2: Initial and Boundary conditions common to P2D model and FHM model [7]

2.2.2 Full homogenised macro-scale (FHM) model

The FHM model consists of two partial differential equations (PDEs) and three algebraic equations as mentioned in table 2.1, while initial and boundary conditions are mentioned in table 2.2. The Li-ion diffusion in the solid phase (electrode) is governed by Fick's law as mentioned in equation (2.1). The boundary conditions are mentioned as follows.

$$\frac{\partial c_{s,j}}{\partial z}\Big\vert_{z=0,L} = 0, \quad \frac{\partial c_{s,j}}{\partial z}\Big\vert_{z=L_n,L_n+L_s} = -\frac{J_j \cdot L_j}{D_{s,j} \cdot F \cdot 3\eta_{s,j}} \tag{2.15}$$

The temperature dependence of the diffusion parameter D_e and reaction rate parameter k_j for the FHM model is shown in the figures 2.4 and 2.5, respectively. The Li-ion diffusion at the collector end of the electrode is zero, as Li-ions can not move to an external circuit. The Li-ion diffusion at the separator end is equivalent to the scaled intercalation

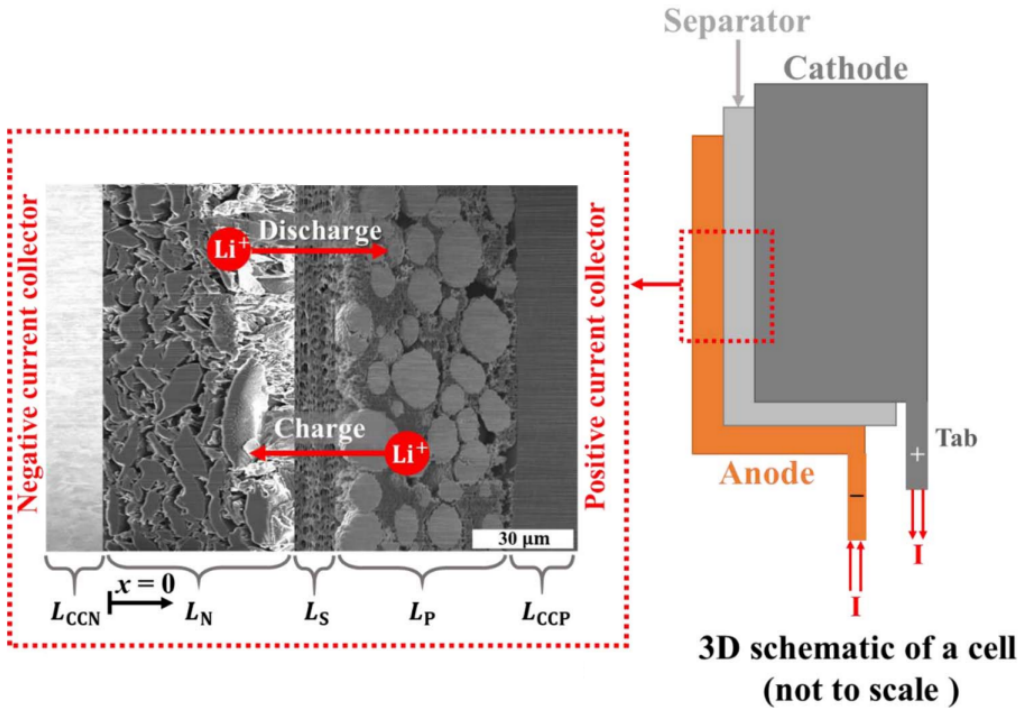

Figure 2.2: Li-ions cell three dimensional schematic [3].

current. The diffusion equation of the FHM model includes the intercalation current J_j as mentioned in the equation 2.1. In contrast, the intercalation current only appears in the boundary condition of the P2D model solid diffusion equation, as mentioned in equation 2.6. The boundary condition at the electrode-separator interface is similar to the corresponding P2D model boundary condition. As the electrode consists of 'fictitious' multiple spherical particles as shown in figure 2.3 [4], variable $R_{s,j}$, i.e. radius of the spherical particles is used in the boundary condition of the P2D electrode model. While the FHM model uses the actual length of the electrode, variable L_j, i.e. length of the electrode, is used in the boundary condition. A three-dimensional schematic of a Li-ion cell obtained from Mehdi's work confirms that the particles in the porous electrode of the Li-ion cell are not spherical, as shown in figure 2.2 [3]. The remaining equations of the FHM model are similar to the P2D model. The value of cell parameters is given in table 2.3 and 2.4.

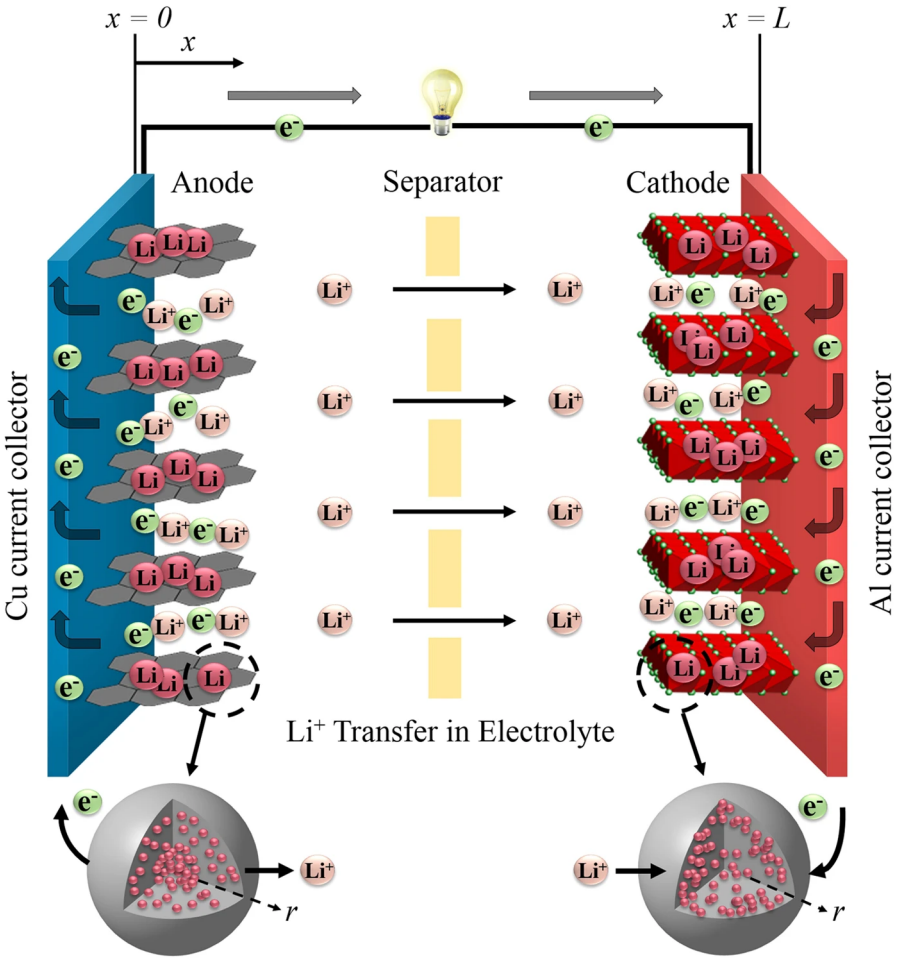

Figure 2.3: Li-ions cell schematic [4].

Name	Symbol	Anode	Cathode	Unit
Thickness	L	53.2	39.9	μm
Particle Radius	R_s	1.2	1.2	μm
Volume Fraction	η	0.626	0.574	-
Conductivity	K_e	113	113	$Amol^{-1}$
Max Concentration	$C_{j,m}$	27088	48700	$mol.m^{-3}$
Stoichiometry	θ	0.7916	0.3494	
Specific Inter-facial Surface Area	a_s	15×10^5	15×10^5	

Table 2.3: Li-ion electrode parameter values [8], [9], [5]

Name	Symbol	value
Capacity	Q	$1.9Ah$
Gas Constant	R	$8.314J.K^{-1}.mol^{-1}$
Reference temperature	T_r	$296K$
Current collector resistance	R_c	0.027Ω
Electrolyte concentration	$C_{e,a}$	$10^3 mol.m^{-3}$
P2D Electrolyte conductivity	K_e	$0.048\Omega m^{-1}$
P2D Electrolyte diffusivity	D_e	$0.99 \times 10^{-11} m^2.s^{-1}$
FHM Electrolyte conductivity	K_e	$0.06\Omega m^{-1}$
FHM Electrolyte diffusivity	D_e	$1.18 \times 10^{-11} m^2.s^{-1}$

Table 2.4: Li-ion cell parameter values[8],[9],[5]

2.3 Simplification of full order electrochemical models

2.3.1 Simplified P2D electrode diffusion model

The simplified electrode diffusion model presented by Subramanian [33] is used in the present work. The following equations describe the approximate solid concentration.

$$\frac{d\bar{c_j}(t)}{dt} = -3\frac{J_j}{a_s \cdot F \cdot R_s} \tag{2.16}$$

$$\frac{D_s}{R_s}[c_{sc,j}(t) - \bar{c_j}(t)] = \frac{-J_j}{5a_s \cdot F} \tag{2.17}$$

The variables $\bar{c_j}(t)$ and $c_{sc,j}$ are the average solid concentration and the surface concentration, respectively. Since the open circuit potential and other variables are functions of the surface concentration $c_{sc,j}$ and state of charge (SoC) is a function of average concentration $\bar{c_j}(t)$, (2.16) and (2.17) are used for simulating the electrode diffusion model.

2.3.2 Simplified FHM electrode diffusion model

We propose that the solid phase concentration along the whole length of an electrode can be approximated by a second-order polynomial, as shown below.

$$c_{s,j}(z,t) = a(t) + b(t)\Big(\frac{z^2}{L_j^2}\Big) \tag{2.18}$$

The value of $c_{s,j}$ from the equation (2.18) is used in the equation (2.15) to obtain the following equation.

$$2\frac{D_{s,j}b(t)}{L_j} = \frac{-J(L_j)\cdot L_j}{3\eta_{s,j}\cdot F} \tag{2.19}$$

The coefficient $b(t)$ can be calculated from the equation (2.19). Another equation is required to find the value of $a(t)$. The following procedure is adopted to solve this problem. The average concentration $\bar{c_j}(t)$ is related to the solid phase concentration.

$$\bar{c_j}(t) = \frac{1}{L_j}\int_{x=0}^{L_j} c_j(z,t)dz \tag{2.20}$$

$$\bar{c_j}(t) = a(t) + \frac{b(t)}{3} \tag{2.21}$$

Averaging both sides of the equation (2.1) gives us the following equation to calculate the average concentration $\bar{c_j}(t)$.

$$\frac{1}{L_j}\int_{z=0}^{L_j}\Big[\frac{\partial c_{s,j}}{\partial t} - D_{s,j}\frac{\partial^2 c_{s,j}}{\partial z^2} + \frac{J(z,t)}{F}\Big]dz = 0 \tag{2.22}$$

$$\frac{d\bar{c_j}(t)}{dt} = -\frac{J(L_j)}{3\eta_{s,j}\cdot F} - \frac{I_{app}}{F\cdot L_j} \tag{2.23}$$

$$I_{app} = \frac{u}{A_c} \tag{2.24}$$

A_c is the surface area of the cell collector. u is the input current. Average concentration $\bar{c_j}(t)$ is calculated using the equation (2.23). The value of unknown time-varying coefficients is calculated using the equations (2.19) and (2.21). The solid phase concentration is calculated using the equation (2.18). The step-wise algorithm is presented in table 2.5.

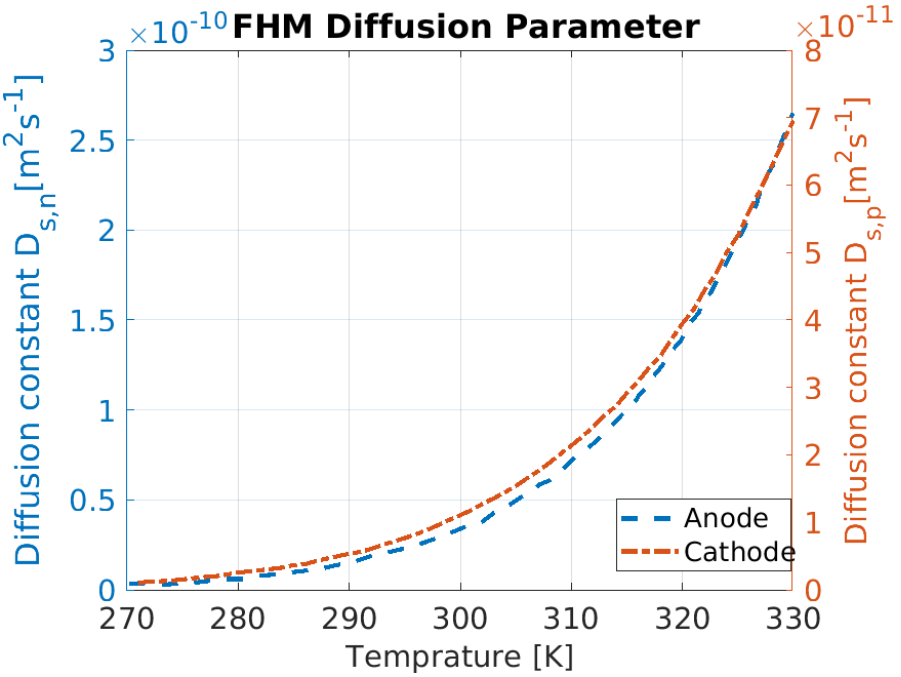

Figure 2.4: Effect of temperature on FHM diffusion parameter is shown in the figure [5].

Step No	Step
1	Available data: Initial discrete time k=0, Initial average Li-ion concentration in electrode $\bar{c_j}(k)$ based on initial SoC.
2	Calculate $\bar{c_j}(k)$ using the equation (2.23)
3	Calculate $b(t)$ using the equation (2.19).
4	Calculate $a(t)$ using the equation (2.21).
5	Calculate solid phase concentration $c_{s,j}(t)$ using the equation (2.18)..
6	Update the value of time k and initial condition $\bar{c_j}(k)$ for next iteration.
7	Repeat step 2 to step 6 for the next sampling instant.

Table 2.5: Algorithm for simplified FHM electrode diffusion model.

2.3.3 Simplified electrolyte diffusion model

The electrolyte diffusion equation (2.2) of the FHM model is simplified by using (2.4).

$$\eta_{e,j}\frac{\partial c_{e,j}(z,t)}{\partial t} = \frac{(1-t_+)J_j(z,t)}{F} + D_{e,j}\frac{\partial^2 c_{e,j}}{\partial z^2} \tag{2.25}$$

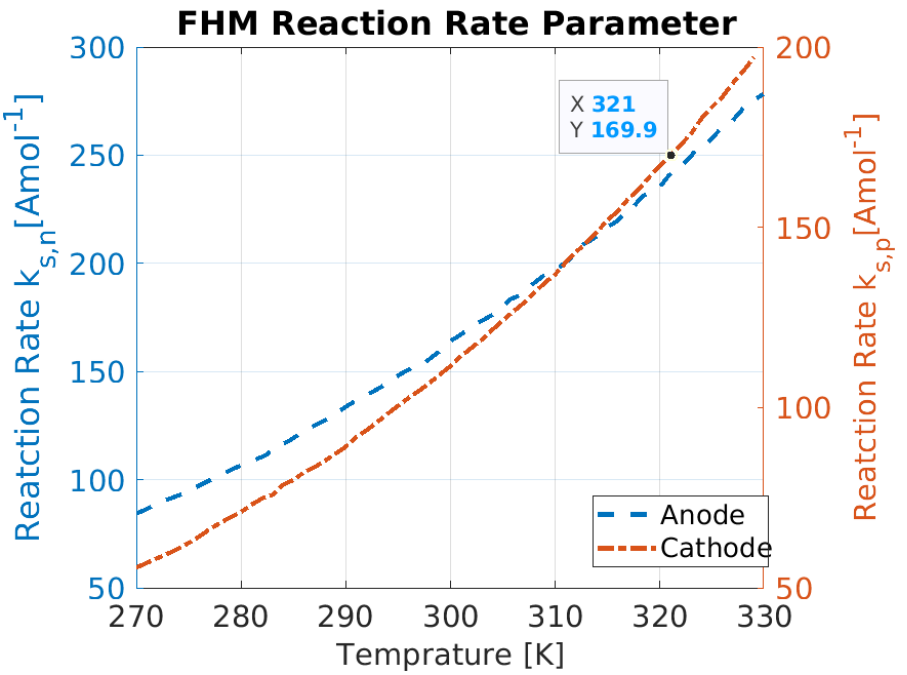

Figure 2.5: Effect of temperature on FHM reaction rate parameter is shown in the figure[5].

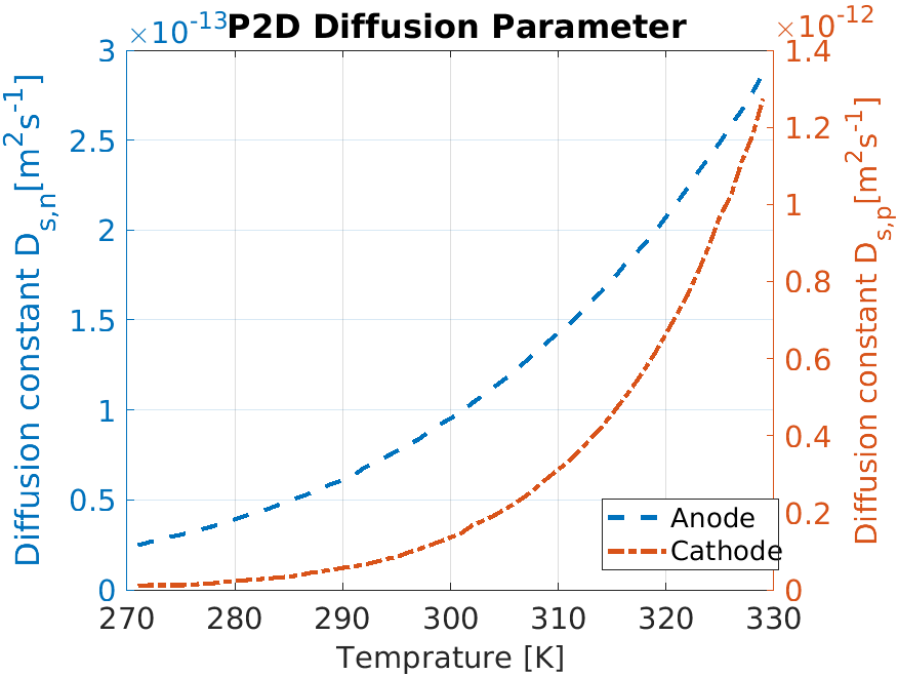

Figure 2.6: Effect of temperature on P2D diffusion parameter is shown in the figure [5].

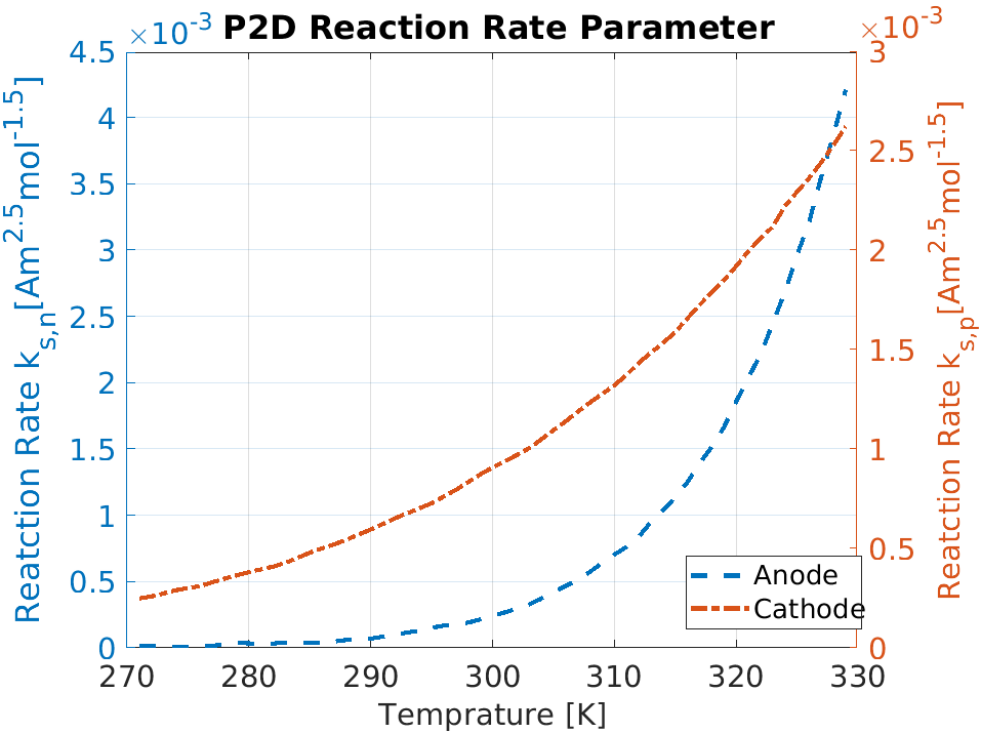

Figure 2.7: Effect of temperature on P2D reaction rate parameter is shown in the figure [5].

The intercalation current term $\frac{(1-t_+)J_j(z,t)}{F}$ is used for electrodes only as electrodes are soaked in electrolyte and Li-ions are constantly moving from electrode to electrolyte and in reverse direction. The intercalation current term is not used for electrolyte equation in separator as Li-ions exists only in the liquid phase and intercalation process can not happen in separator as shown in figure 2.1 and 2.3. FHM electrolyte diffusion equation (2.25) is similar to the P2D electrolyte diffusion equation. The method in [10], and [2] is used to simplify FHM liquid phase (electrolyte) diffusion equation. Li-ion concentration in the three regions, i.e. anode, separator and cathode, is approximated by a second-order polynomial as given below.

$$c_{e,n}(z) = a_1 z^2 + a_0, \;\; 0 \leq z \leq L_n \tag{2.26}$$

$$c_{e,s}(z) = a_4 z^2 + a_3 z + a_2, \;\; 0 \leq z \leq L_s \tag{2.27}$$

$$c_{e,p}(z) = a_6 z^2 + a_5, \;\; 0 \leq z \leq L_p \tag{2.28}$$

The first-order term in the equations (2.26) and (2.28) is zero due to the boundary condition mentioned in the equation (2.12). The following four equations are derived by putting the value of $c_{e,j}(z)$ in the continuity conditions given by the equation (2.13).

$$a_1 L_n^2 + a_0 = a_2 \tag{2.29}$$

$$a_6 L_p^2 + a_5 = a_4 L_s^2 + a_3 L_s + a_2 \tag{2.30}$$

$$2a_1 L_n D_{e,n} = a_3 D_{e,s}^{eff} \tag{2.31}$$

$$-2a_6 L_p D_{e,p} = (2a_4 L_s + a_3) D_{e,s} \tag{2.32}$$

The total amount of Li-ions in the anode, separator and cathode $Q_{e,j}$ is calculated by integrating the equations (2.26), (2.27) and (2.28) respectively.

$$Q_{e,n}(t) = \eta_{e,n} \int_0^{L_n} c_{e,n}(z) dz = \eta_{e,n} \left(\frac{a_1 L_n^3}{3} + a_0 L_n \right) \tag{2.33}$$

$$Q_{e,s}(t) = \eta_{e,s} \int_0^{L_s} c_{e,s}(z) dz = \eta_{e,s} \left(\frac{a_4 L_s^3}{3} + \frac{a_3 L_s^2}{2} + a_2 L_s \right) \tag{2.34}$$

$$Q_{e,p}(t) = \eta_{e,p} \int_0^{L_p} c_{e,p}(z) dz = \eta_{e,p} \left(\frac{a_6 L_p^3}{3} + a_5 L_p \right) \tag{2.35}$$

We calculate derivatives of $Q_{e,j}$ subject to electrolyte boundary and continuity conditions to obtain the following equations.

$$\begin{aligned} \frac{d}{dt} Q_{e,n}(t) &= \frac{I_{app}(1 - t_+)}{F} + D_{e,n} \frac{\partial c_{e,n}}{\partial z} \Bigg|_{z=0}^{z=L_n} \\ \frac{d}{dt} Q_{e,n}(t) &= \frac{I_{app}(1 - t_+)}{F} + D_{e,n} 2a_1 L_n \end{aligned} \tag{2.36}$$

$$\begin{aligned} \frac{d}{dt} Q_{e,p}(t) &= \frac{I_{app}(1 - t_+)}{F} + D_{e,p} \frac{\partial c_{e,p}}{\partial z} \Bigg|_{z=0}^{z=L_p} \\ \frac{d}{dt} Q_{e,p}(t) &= -\frac{I_{app}(1 - t_+)}{F} + D_{e,p} 2a_6 L_p \end{aligned} \tag{2.37}$$

$$\frac{d}{dt}Q_{e,s}(t) = D_{e,s}\frac{\partial c_{e,s}}{\partial z}\Big|_{z=0}^{z=L_s}$$
$$\frac{d}{dt}Q_{e,s}(t) = D_{e,s}2a_4L_s \tag{2.38}$$

The seven unknown coefficients are solved using the seven equations, i.e. (2.29), (2.30), (2.31), (2.32), (2.36), (2.37) and (2.38). The equations (2.26),(2.27) and (2.28) are used to simulate the electrolyte diffusion model. Step-wise algorithm is provided in table 2.6.

Step No	Step
1	Available data:Initial discrete time k=0, Initial total concentration of Li-ions in electrolyte $\bar{Q_{e,j}}(0)$ based on initial concentration.
2	Calculate $a_0, a_1 ... a_6$ using the equations (2.29), (2.30), (2.31), (2.32), (2.36), (2.37) and (2.38) .
3	Calculate total Li-ion concentration $Q_{e,j}(k)$ at next time instant using the equations (2.26),(2.27) and (2.28).
4	Update the value of time k and initial condition $Q_{e,j}(k)$ for the next iteration.
5	Repeat step 2 to step 6 for the next sampling instant.

Table 2.6: Algorithm for the simplified electrolyte diffusion model [10], [2] .

2.3.4 Approximation of intercalation current

The intercalation current J_j is assumed constant. The following equations are derived using the equation (2.4).

$$J_n = \frac{I_{app}}{L_n \cdot F}$$
$$J_p = \frac{-I_{app}}{L_p \cdot F} \tag{2.39}$$

This model is called the Further simplified FHM model.

2.3.5 Simplification of algebraic equations

Approximation for the algebraic equation of Li-ion cell is based on the work of S. J. Moura [80]. The intercalation current J_j is assumed constant. Exchange current density $i_0(x,t)$ is approximated by the spatial average value $\bar{i_o}(t)$ and approximate over-potential $\bar{\eta}$ is given by the following equation.

$$\bar{\eta}(t) = \frac{RT}{\alpha F} sinh^{-1}\Big(\frac{I_{app}}{2\alpha L \bar{i}_{0,j}}(t)\Big) \tag{2.40}$$

$$V = \phi_{s,p}(L) - \phi_{s,n}(0) \tag{2.41}$$

$$\phi_{s,j}(z,t) = \bar{\eta_j} + \phi_{e,j}(x,t) + U_{c,j}(z,t) \tag{2.42}$$

The procedure mentioned in ref. [80] is used to simplify the output voltage and potential equation. The simplified output voltage equation is mentioned as follows.

$$\begin{aligned} V = \bar{\eta_p}(t) - \bar{\eta_n}(t) + U_p(\theta(L)) - U_n(\theta(L)) + \\ k_1 I_{app} + k_2(\ln(c_e(L)) - \ln(c_e(0))) \end{aligned} \tag{2.43}$$

$$k_1 = \frac{L_n + 2L_s + L_p}{2K_{eff}} \tag{2.44}$$

$$k_2 = \frac{2RT(1-t_+)K_{eff}}{F} \tag{2.45}$$

This model is labelled as SFHM 2 model.

2.4 Numerical implementation using orthogonal collocation

2.4.1 Spatial discretisation

Spatial discretisation is done using orthogonal collocation developed by Adrien [42]. The following equation describes the solution $u_e(\gamma,t)$ of a PDE.

$$u_N(\gamma,t) = \sum_{j=0}^{N} \hat{u}_j(t)\phi_j(\gamma), \qquad \gamma\epsilon[-1,1] \tag{2.46}$$

$$\phi_j(\gamma) = \frac{(-1)^{j+1}(1-\gamma^2)T_N^r(\gamma)}{\bar{c}_w N^2(\gamma-\gamma_i)}, \qquad \gamma\epsilon[-1,1] \tag{2.47}$$

$\bar{c}_j = 0$ for $j = 0, N$ and $\bar{c}_w = 1$ otherwise $T_N(\gamma)$ denotes the Chebyshev polynomial of degree N. $\hat{u}_j(t)$ is equal to the value of solution $u_e(\gamma_i, t)$ at discretised nodes known as collocation points. The following equation gives the collocation points.

$$\gamma_i = cos\Big(\frac{\pi i}{N}\Big), \qquad i = 0, 1..M. \tag{2.48}$$

M is the maximum number of collocation points. The p^{th} derivative of $u_e(\gamma, t)$ at collocation points is calculated as follows.

$$u_N^p(\gamma_i) = \sum_{j=0}^{M} d_{i,j}^p u_N(\gamma_i) \tag{2.49}$$

$d_{i,j}^p$ is calculated by finding the derivative of the function $\phi_j(\gamma)$. Chebyshev polynomials are computed offline and stored to reduce the computational burden. The derivative equation is written in matrix form as follows.

$$\mathbf{u}^p = D_N^p \mathbf{u} \tag{2.50}$$

Similarly, integration or quadrature of $u(\gamma, t)$ is calculated as follows.

$$u_N^p(\gamma_i) = \sum_{j=0}^{N} \alpha_{i,j} u_N(\gamma_i) \tag{2.51}$$

$\alpha_{i,j}$ is calculated by finding the integration or quadrature of the function $\phi_j(\gamma)$. MATLAB ®functions for the differentiation matrix and integration matrix provided by [82] are used in this work.

2.4.2 Temporal discretisation

Average solid concentration in anode $\bar{c_n}(t)$ and cathode $\bar{c_p}(t)$ and total liquid concentration in anode $Q_{e,n}$, separator $Q_{e,s}$ and cathode $Q_{e,p}$ are states of the nonlinear state space model (i.e. simplified FHM model) of Li-ion cell. Equations (2.23),(2.36), (2.37)

and (2.38) are dynamic equations of the simplified model as the time derivative of states is given by these equations. The equations can be grouped and represented as follows:

$$\dot{x}(t) = f(x(t), u(t)) \tag{2.52}$$

The output equation is represented as follows.

$$y = g(x, u) \tag{2.53}$$

f, x, u, y and g are state function, system states, input current, output variable, and output function, respectively. Solid and liquid concentration variables are considered the state variables of the cell. Current is considered as the input. Cell voltage and SoC are considered output. The following equation calculates SoC of the cell using anode solid Li-ion concentration.

$$SoC(t) = \frac{\theta^{avg}(t) - \theta_n^{0\%}}{\theta^{100\%} - \theta^{0\%}} \tag{2.54}$$

The following equation calculates the normalised average concentration of anode for the P2D model and FHM model.

$$\theta^{avg}(t) = \frac{3}{L_j R_{s,j}^3} \int_0^{L_j} \int_0^{R_{s,j}} r^2 \frac{c_{s,j}(z, r, t)}{c_{j,m}} dr dz \tag{2.55}$$

$$\theta^{avg}(t) = \frac{1}{L_j} \int_0^{L_j} \frac{c_{s,j}(z, t)}{c_{j,m}} dz \tag{2.56}$$

$\theta_j^{0\%}$ and $\theta_j^{100\%}$ denote 0% and 100% SoC respectively and mentioned in the table 2.3. The equation is discretised using orthogonal collocation. The details of orthogonal collocation are discussed in section 2.4. The n dimensional matrix equation corresponding to n collocation points is expressed as follows.

$$X_{N\times 1} = X(t_0)_{N\times 1} + \frac{t_f - t_0}{2} A_{N\times N} F_{N\times 1}(X, U) \tag{2.57}$$

$A_{N\times N}$ is the pseudos-spectral integration matrix. t_0 and t_f are the initial and final times, respectively. The value of state matrix F is given as follows.

$$F = \begin{bmatrix} -\frac{J(L_n)}{3\eta_s \cdot F} - \frac{I_{app}}{F \cdot L_n} \\ -\frac{J(L_p)}{3\eta_s \cdot F} - \frac{I_{app}}{F \cdot L_p} \\ \frac{I_{app}(1-t_+)}{F} + D_{e,n} 2a_1 L_n \\ -\frac{I_{app}(1-t_+)}{F} + D_{e,p} 2a_6 L_p \\ D_{e,s} 2a_4 L_s \end{bmatrix} \tag{2.58}$$

The output equation (2.43) is an algebraic equation. The following equation represents the output equation in matrix form.

$$Y_{N\times 1} = G_{N\times 1}(X, U) \tag{2.59}$$

The value of output matrix G for voltage output is given as follows.

$$\begin{aligned} G = \bar{\eta_p}(\gamma_i) - \bar{\eta_n}(\gamma_i) + U_{c,p}(\theta(L)) - U_{c,n}(\theta(0)) + \\ k_1 I_{app} + k_2(\ln(c_e(L)) - \ln(c_e(0))) \end{aligned} \tag{2.60}$$

γ_i is the collocation point or discretised time.

2.5 Results and discussion

Simulation results are produced using MATLAB. Crank-Nicolson is used for the discretisation of models to produce results shown in figures 2.8,2.10,2.9,2.11 and table 2.7. Whereas MATLAB function Ode15s and orthogonal collocation is used to produce results shown in table 2.8 and figure 2.12. Parameters are primarily obtained from [41], [7], [6]. The sampling time is 1 second, and the cell temperature is 318K. The percentage root mean square (RMS) error between the voltage V_i and the reference voltage $V_{ref,i}$ is calculated using the following equation to quantify the accuracy of a particular voltage signal V_i.

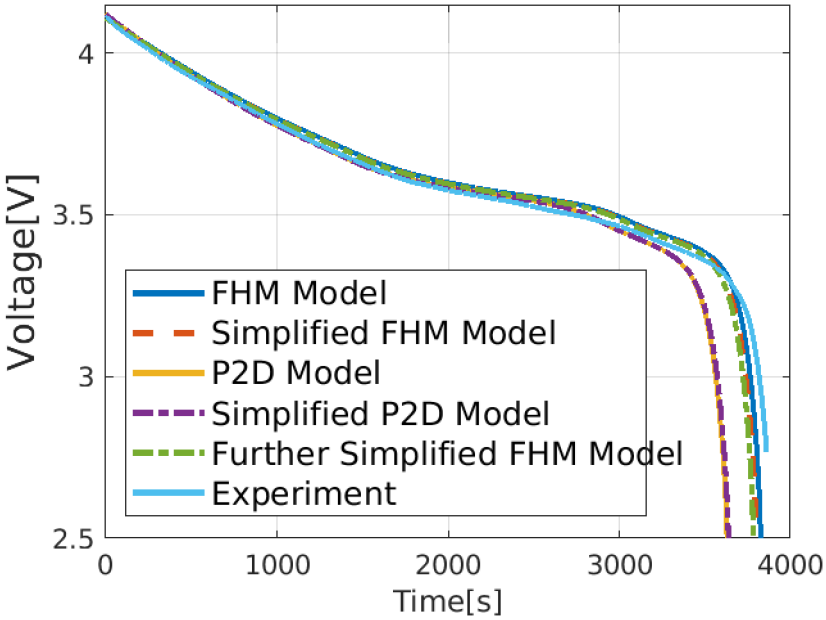

Figure 2.8: Output voltage of various Li-ion cell models for $1C$ input current at 318K temperature.

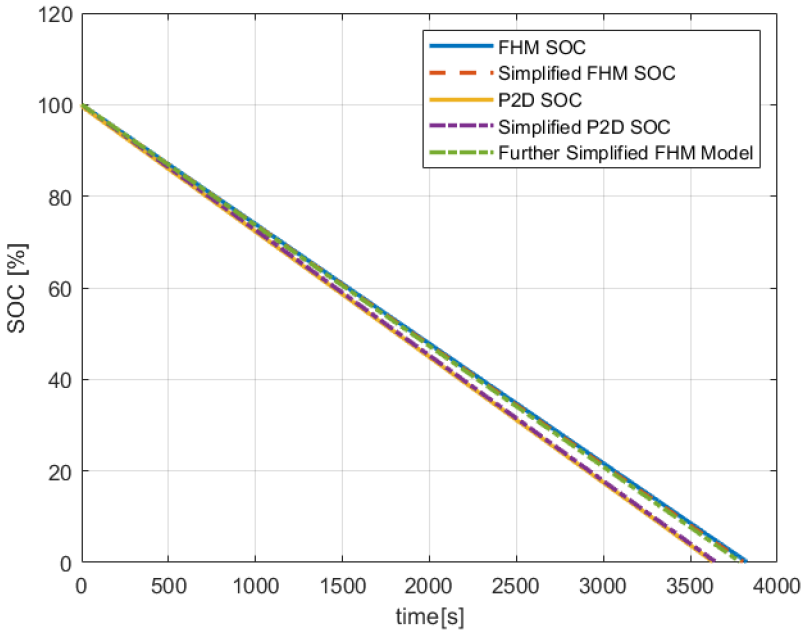

Figure 2.9: SoC of various Li-ion cell models for $1C$ input current at 318K temperature.

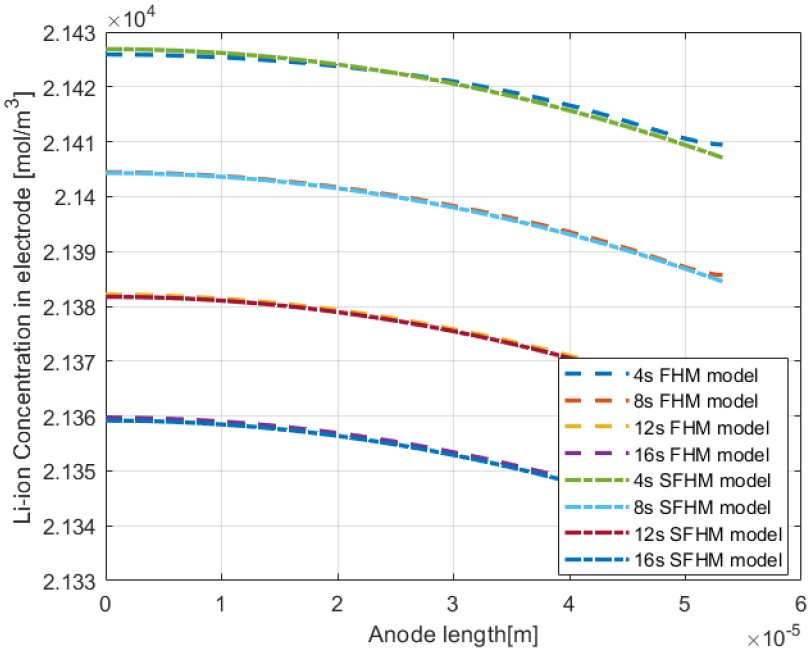

Figure 2.10: Li-ion concentration profile vs the length of anode for FHM model and SFHM model for $1C$ current input at $4, 8, 12$ and 16s.

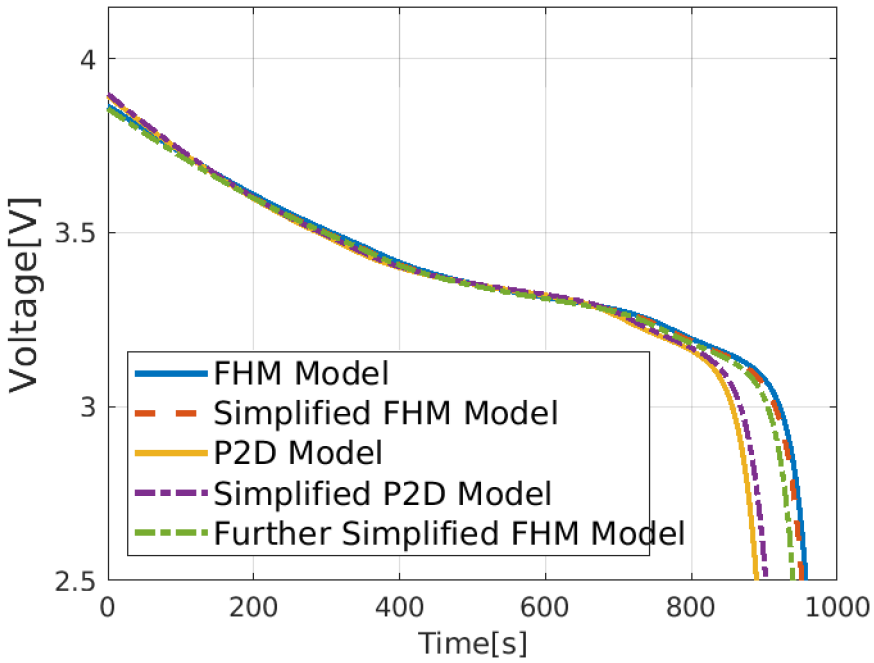

Figure 2.11: Output voltage of various Li-ion cell models for $4C$ input current at 318K temperature.

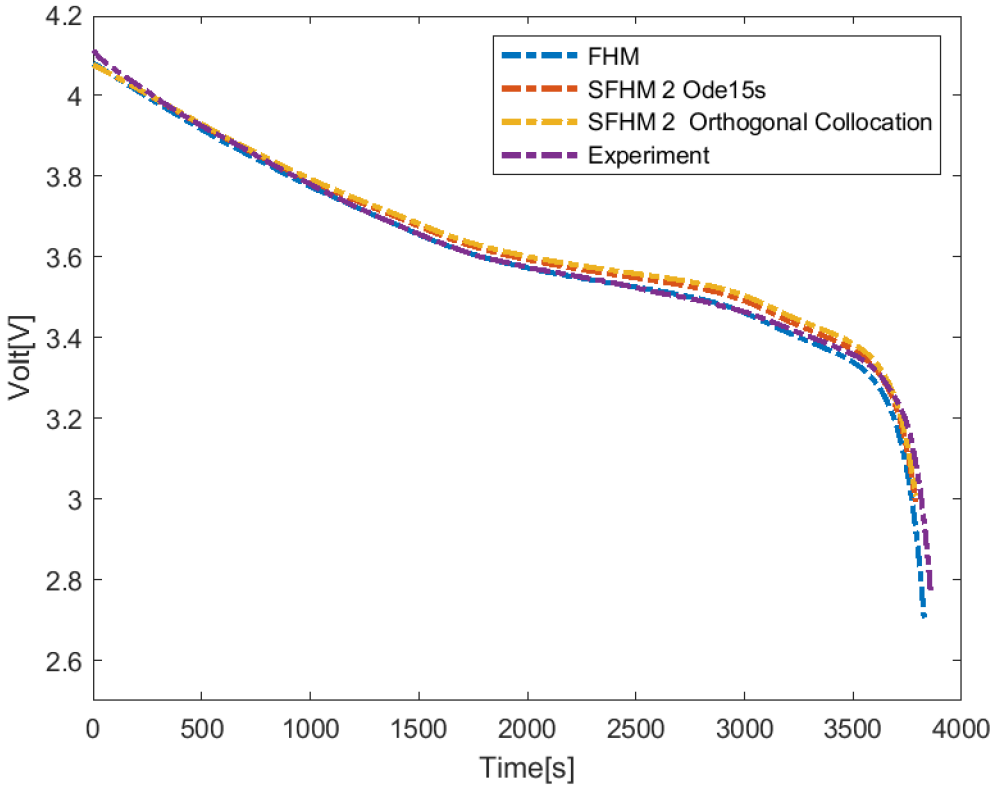

Figure 2.12: Comparison of output voltage for FHM model, SFHM 2 model, and experiment at $1C$ current input at 318K temperature. Experimental results are obtained from [6]

$$RMS\ Error = \frac{100}{mean(V_{ref})} \times \sqrt{\frac{1}{N}\sum_{i=0}^{N}(V_{ref,i} - V_i)^2} \tag{2.61}$$

The experimental voltage is taken as a reference for calculating RMS error. Experimental results are obtained from Harikesh's article[6]. Considering figure 2.8, we observe that at 318K, the performance of the FHM model and the proposed simplified FHM model is excellent, and the value of RMS error is 0.6% for $1C$ current. Compared to the FHM model and the simplified FHM model, the P2D model and the simplified P2D model show relatively inaccurate performance. The value of RMS error for the P2D and the simplified P2D model is about 2% for $1C$ current. Consider figure 2.8, it can be observed that the high value of RMS error for the P2D model and the simplified P2D model is mainly due to performance deterioration at low values of SoC. We also observe that the output voltage of the simplified FHM model and simplified P2D model accurately track the output of the FHM model and the P2D model, respectively.

Consider figure 2.8; we observe that SoC estimation using the simplified P2D model is not accurate while the simplified FHM model accurately estimates SoC.

Figure 2.10 shows the Li-ion concentration for the FHM model and simplified FHM model in anode at various time instants. This plot is the same as the plot of the second-order polynomial, i.e. parabola $p(x) = ax^2 + bx + c$ where x represents the physical dimension of the electrode. Based on this fact, our assumption of approximating the Li-ion concentration for the FHM electrode equation using a second-order polynomial is proved correct. The same plot is observed for both electrodes at all points in time. The same observations are recorded for electrolyte, which justifies the use of quadratic polynomial for the approximation of liquid phase concentration.

The main reason for the superior performance of the FHM model and the simplified FHM model is that the FHM model is derived based on the actual structure of the electrode. In contrast, the P2D model is derived based on the assumption that fictitious spherical particles constitute an electrode. For the FHM model, the value of temperature-dependent parameters, such as the electrode diffusion parameter and the reaction rate constant, is calculated based on the numerical modelling of the electrode structure. The P2D model uses the empirical and relatively inaccurate Bruggeman method. We observe

that the RMS error of the further simplified FHM model is equal to the RMS error of the simplified FHM model for $1C$ current, as shown in table 2.7. However, when the input current is increased to $4C$, the error for a further simplified FHM model is increased to 3%, and the error for a simplified FHM model is 2.1% considering FHM voltage output as a reference signal. The result is shown in figure 2.11.

Consider table 2.7, the algorithm execution time for the FHM model is 34s, less than the P2D model execution time, i.e. 62s as the FHM model has only one dimension, and the P2D model has additional pseudo dimension for electrode particles. The proposed simplified FHM reduced the algorithm execution time by 35% to 20s, slightly less than the simplified P2D model's algorithm execution time, i.e. 21s. Further simplifying the FHM model slightly reduces the algorithm execution time to 19s. The proposed simplified FHM model can accurately track the output voltage of the FHM model up to $4C$ current with 2.1% RMS error considering FHM voltage as a reference as shown in figure 2.11 and table 2.9.

Figure (2.12) compares the output voltage obtained from the experiment with the output voltage predicted using various models, i.e. the FHM model, SFHM 2 model. Experimental results are obtained from [6]. Initial and final SoC is set to 99.9% and 0.1% respectively. The sampling time is 1 second. The cell is discharged at $1C$ current and 318K temperature. SFHM model is simulated using MATLAB Odes15s function and orthogonal collocation. Other models are simulated using the Ode15s function.

Table (2.8) compares the root mean square error (RMS) and algorithm execution time per iteration between the experimental output voltage and the predicted output voltage for each model. The output voltage predicted by the SFHM 2 model using the Ode15s function and orthogonal collocation has an approximation RMS error of 1.31% and 1.28%. The models predict the output voltage with an approximation error greater than the SFHM model. The greater error is the price paid for further simplification.

Consider the algorithm execution time of various models at $1C$ discharging current mentioned in table (2.8). The orthogonal collocation is about 18 times faster than the ode15s function. Based on this discussion, we conclude that the simplified FHM model variants combine the accurate estimation property of the FHM model and the

low algorithm execution time property of the simplified P2D model, making it a good candidate for developing BMS.

Model	Algorithm execution time	RMS Error
FHM model	$34s$	0.6%
P2D model	$62s$	2%
Simplified FHM model	$20s$	0.6%
Simplified P2D model	$21s$	2%
Further simplified FHM model	$19s$	0.6%

Table 2.7: Comparison of algorithm execution time and RMS error for various Li-ion cell models for $1C$ current at 318K temperature.

Model	Method	RMS Error	Algorithm execution time (seconds)
FHM	Ode15s	0.5%	21s
SFHM 2	Ode15s	1.31%	1.5s
SFHM 2	Orthogonal collocation	1.28%	0.08s

Table 2.8: Comparison of root mean square error (RMS) and algorithm execution time for the FHM model and SFHM 2 model using various discretisation techniques at $1C$ current input at $318K$ temperature.

Model	Method	RMS Error	Algorithm execution time(seconds)
SFHM	Ode15s	2.1%	1.21s
SFHM 2	Ode15s	3%	1.2s

Table 2.9: Comparison of voltage root mean square error (RMS) and algorithm execution time for the FHM model, SFHM Model and SFHM 2 model considering the FHM model as a reference model. The input current is $4C$, and the temperature is 318K.

Chapter 3

Optimal charging of a Li-ion cell

3.1 Introduction of optimal charging

A charging strategy is vital to charge a Li-ion cell quickly, efficiently and safely. Charging algorithms are classified into two categories, i.e. model-free charging algorithms and model-based charging algorithms. Both methods are discussed briefly.

Model-free charging methods do not consider a Li-ion cell's internal dynamics. A cell's input current and output voltage are the only quantities of interest for developing these charging methods. The most well-known model-free charging algorithm is the constant current constant voltage ($CCCV$) charging algorithm. $CCCV$ is the industry standard optimal charging algorithm for a Li-ion cell. In this charging technique, a cell is initially charged at a constant current until the cell output voltage reaches a maximum threshold. This charging phase is called the CC charging phase. Afterwards, the cell is charged at the maximum voltage. The charging current gradually decreases and diminishes in CV charging mode.

Other well-known model-free charging techniques are multi-step charging and pulse charging. In the multi-step charging technique, the charging phase is divided into multiple phases, with a distinct value of constant input current charges each. The pulse charging algorithm feeds the battery by input current pulses of distinct amplitude, duty cycle, and frequency. The details of model-free charging algorithms are available in literature [83]. However, model-free algorithms are not the best to optimise a Li-ion

cell's health as their design is not based on the battery model. The model-free charging algorithm is designed based on the physical quantities of cells that are either input or output, i.e. input current or output voltage.

Model-based charging algorithms are better candidates to minimise health loss as the charging algorithm is aware of cell dynamics, the conditions and the parameters or quantities of cells that affect the health of a cell. The charging regimes that optimise the health-defining parameters of a cell can be employed using this charging method; thus, the damage to the cell's health can be minimised.

Numerous model-based charging algorithms have been explored using either equivalent circuit models or simplified electrochemical models recently; for example, Hu *et al.*, Sun *et al.* and Drees *et al.* have proposed charging algorithms using equivalent circuit models [54], [84], [85]. Klein *et al.*, Yang *et al.*, Khalik *et al.*, Liu *et al.* and Malik *et al.* have proposed electrochemical model-based health-conscious charging algorithms to reduce cell ageing. [62], [54], [52],[53], [86].

The novel contribution of this work includes pseudo-spectral optimal control of a Li-ion cell using a simplified FHM model. The solid electrolyte interphase (SEI) layer model mentioned in [56], [63], and [57] is incorporated in the simplified FHM model to make the charging algorithm health-conscious. The capacity fade of a Li-ion cell is also studied. The state of health (SoH) definition is not unique, as multiple factors degrade the battery's health. We have used a definition of SoH based on capacity degradation or capacity fade.

The so-called direct approach solves the optimal control problem (OCP). The continuous-time OCP is converted to a nonlinear programming problem (NLP) using orthogonal collocation on Chebyshev polynomials. The NLP is solved using well-known NLP-solving algorithms such as the active set method. We have used MATLAB command *fmincon* to solve the NLP. The control problem is to charge a Li-ion cell with minimum health degradation in minimum time subject to input, state and output constraints. Model predictive control is implemented for optimal charging. Both control objectives, i.e. minimum charging time and minimum health degradation, comprise the cost function of MPC. The performance of the health-conscious control algorithm is compared with the

industry-standard CCCV charging algorithm.

The comparison between the health-conscious charging algorithm and the *CCCV* algorithm using the simplified FHM model shows that the health-conscious charging algorithm outperforms the *CCCV* algorithm by reducing the degradation in film resistance R_{film} and SoH. The performance of the algorithms is analysed and compared under various conditions. For example, the performance is analysed by the varying value of input current constraint and cost function weighting factor. The performance of algorithms is also compared for multiple-cycle charging.

This chapter is organised as follows. Section 3.2 briefly describes the simplified FHM model. Pseudo-spectral optimal control is discussed in section 3.3.1. Section 3.4 presents results, analysis and discussion.

3.2 Mathematical modelling of a Li-ion cell

The details of mathematical modelling are given in the modelling chapter and literature [87]. Here, we briefly discuss the solid electrolyte inter-phase model.

3.2.1 Solid Electrolyte Inter-phase (SEI) Layer Model

Side reaction in negative electrode increases resistivity R_{film} to Li-ion flow and is the primary cause of cell ageing in graphite negative electrodes. The SEI layer model proposed by Ramadass et al.[56] and Safari et al.[57] is used in this work with some modifications. Values of parameters related to the SEI layer model are mentioned in [56] and [57].

The SEI layer model is coupled to the cell model. We assume that besides anode intercalation current J_n side reaction flux density J_s also contributes toward molar flux density J_{total} of Li-ions:

$$J_{total} = J_n + J_s \tag{3.1}$$

The side reaction molar flux is described by a $Tafel$ equation which by definition relates the overpotential to the side reaction as mentioned below:

$$J_s = -i_{0,s} e^{\frac{RT}{\alpha F}\eta_s} \tag{3.2}$$

$i_{0,s}$ is the side reaction exchange current density and η_s is the side reaction over potential expressed by the following equation:

$$\eta_s = \eta_n + U_{c,n}(\theta) - U_{ref,s} \tag{3.3}$$

$U_{ref,s}$ is the side reaction open circuit potential. The following equation describes film resistance formed on the negative electrode due to side reaction molar flux:

$$\frac{\partial R_{film}}{\partial t} = \frac{-i_{0,s} M_p}{\kappa_p \rho_p F} e^{\frac{RT}{\alpha F}\eta_s} \tag{3.4}$$

M_p, κ_p and ρ_p are molecular weight, electrolyte conductivity, and density of products formed due to side reactions, respectively. The following equation describes the capacity loss of Li-ion cell:

$$\frac{\partial Q}{\partial t} = \int_0^{L_{neg}} A_c J_s dx \tag{3.5}$$

Q is the capacity of a Li-ion cell. State of health (SoH) is defined as normalised capacity loss expressed in percentage as mentioned below:

$$SoH = \frac{Q}{Q_{nominal}} \times 100\% \tag{3.6}$$

3.3 Pseudo-spectral Optimal Control

3.3.1 Orthogonal Collocation

Spatial discretisation of the FHM model is achieved using orthogonal collocation developed by Adrien [42]. The exact solution $u_e(\gamma)$ of an ODE is approximated by variable

$u_N(\gamma)$ using Chebyshev polynomials as shown next:

$$u_N(\gamma) = \sum_{j=0}^{N} \hat{u}_j(\gamma_i)\phi_j(\gamma), \qquad \gamma\epsilon[-1,1] \tag{3.7}$$

N is the highest order of the Chebyshev polynomial. Subscript j is an index variable for Chebyshev polynomials. t is the time variable. For using orthogonal collocation, we have to re-scale the independent variable, i.e. time signal t, from its full range to the range of collocation variable γ, i.e. from -1 to 1.

$$\phi_j(\gamma) = \frac{(-1)^{j+1}(1-\gamma^2)T_N(\gamma)}{\bar{c}_j N^2(\gamma-\gamma_i)}, \qquad \gamma\epsilon[-1,1] \tag{3.8}$$

$\bar{c}_j = 0$ for $j = 0, N$ and $\bar{c}_j = 1$ otherwise $T_N(\gamma)$ denotes the Chebyshev polynomial of degree N. $\hat{u}_j(t)$ is equal to the value of exact solution $u_e(\gamma_i)$ at discretised time signal known as collocation points. Although the exact solution is unknown, the solution's value at collocation points is known. The following equation gives the collocation points:

$$\gamma_i = cos\Big(\frac{\pi i}{N}\Big), \qquad i = 0, 1...N. \tag{3.9}$$

Subscript i is the index variable for collocation points. The p^{th} derivative of the exact solution $u_e(\gamma)$ at collocation points is approximated by calculating the derivative of Chebyshev polynomials. As Chebyshev polynomials are already known, the derivative can be pre-calculated as follows.

$$u_N^p(\gamma_i) = \sum_{j=0}^{N} d_{i,j}^p u_N(\gamma_i) \tag{3.10}$$

$d_{i,j}^p$ is calculated by finding the derivative of the function $\phi_j(\gamma)$. Since Chebyshev polynomials are already known, they are computed offline to reduce the online computational burden. The derivative equation is written in matrix form as follows:

$$\mathbf{u}^p = D_N^p \mathbf{u} \tag{3.11}$$

Integration or quadrature of $u_e(\gamma)$ is also calculated using the same method. Trefethen [88] and Reddy [89] have provided MATLAB algorithms and codes to generate the differentiation and integration matrix using orthogonal collocation, and we have used it in current work.

3.3.2 Nonlinear Programming Problem Formulation

Average solid concentration in anode $\bar{c_n}(t)$ and cathode $\bar{c_p}(t)$ and total liquid concentration in anode $Q_{e,n}$, separator $Q_{e,s}$ and cathode $Q_{e,p}$ are states of the nonlinear state space model (i.e. simplified FHM model) of Li-ion cell. Equations (2.23), (2.36), (2.37) and (2.38) are dynamic equations of the simplified model as the time derivative of states is given by these equations. The equations can be grouped and represented as follows:

$$\dot{x}(t) = g(x(t), u(t)) \tag{3.12}$$

Output equation (2.43) is an algebraic equation and is represented as follows.

$$y = h(x, u) \tag{3.13}$$

g, x, u, y and h are state function, states, input, output variable, and output function, respectively. Solid and liquid concentration variables are considered the state variables of the cell. Current is considered as the cell input. Cell voltage and SoC are considered output. SoC (using Li-ion concentration in anode) is calculated by the following equation:

$$SoC(t) = \frac{\theta^{avg}(t) - \theta^{0\%}}{\theta^{100\%} - \theta^{0\%}} \tag{3.14}$$

The following equation calculates the normalised average concentration:

$$\theta^{avg}(t) = \frac{1}{L_n} \int_0^{L_n} \frac{c_{s,n}(x,t)}{c_{n,m}} dx \tag{3.15}$$

$c_{s,n}$ is the Li-ion concentration in anode. $c_{n,m}$ is the maximum Li-ion concentration in anode. $\theta^{0\%}$ and $\theta^{100\%}$ denote 0% and 100% SoC respectively. We have used the anode to define SoC of the cell as the anode concentration is gradually reduced by SEI layer

formation.

The equation is discretised using orthogonal collocation. The details of orthogonal collocation are discussed in section 3.3.1. The N dimensional matrix equation corresponding to N collocation points is expressed as follows:

$$X_{N\times 1} = X(t_0)_{N\times 1} + \frac{t_f - t_0}{2} A_{N\times N} G_{N\times 1}(X, U) \tag{3.16}$$

t_0 is the initial time. t_f is the final time. The above equation gives values of states at N collocation points between t_0 and t_f. $A_{N\times N}$ is the integration matrix. Value of state matrix G is given as follows:

$$G = \begin{bmatrix} -\frac{J(x_N)}{3\eta_s \cdot F} - \frac{I_{app}}{F \cdot L_n} \\ -\frac{J(x_N)}{3\eta_s \cdot F} - \frac{I_{app}}{F \cdot L_p} \\ \frac{I_{app}(1-t_+)}{F} + D_{e,n} 2a_1 L_n \\ -\frac{I_{app}(1-t_+)}{F} + D_{e,p} 2a_6 L_p \\ D_{e,s} 2a_4 L_s \end{bmatrix} \tag{3.17}$$

Equation (2.43) is an algebraic equation. The following equation represents it in matrix form:

$$Y_{N\times 1} = H_{N\times 1}(X, U) \tag{3.18}$$

The output matrix H for voltage output Y is as follows.

$$H = \bar{\eta_p}(\gamma_i) - \bar{\eta_n}(\gamma_i) + U_{c,p}(\theta(\gamma_N)) - U_{c,n}(\theta(\gamma_0)) + k_1 I_{app} + k_2(\ln(c_e(\gamma_N)) - \ln(c_e(\gamma_0))) \tag{3.19}$$

γ_i is the collocation point or discretised time.

CCCV charging algorithm is the industry standard charging algorithm to charge Li-ion cells. *CCCV* charging of a Li-ion cell using the SPM is extensively studied, as mentioned in the introduction. Liu [52] and Malik [53] have compared the *CCCV* charging algorithm with their proposed health-conscious charging algorithm. For the

$CCCV$ charging, the battery cell is first charged using a constant current up to a certain voltage threshold, followed by constant voltage charging. The cost function of $CCCV$ charging algorithm is mentioned below:

$$\min_u J_c = \min_u \int_{t_0}^{t_f} (SoC_{ref} - SoC)^2 dt \tag{3.20}$$

SoC_{ref} is 100%. The terminal cost is assumed to be zero. The term in the cost function is included to track reference SoC with minimum error. The discretised cost function is given as follows:

$$\min_u J_c = \min_u \frac{t_f - t_0}{2} \Big[\sum_{i=0}^{P_H} (SoC_{ref} - SoC(\gamma_i))^2 \alpha_i \Big] \tag{3.21}$$

α_i is the quadrature weight. P_H is the prediction horizon.

The optimisation problem is to find the value of the input current u to minimise a cost function J_c such that (3.16) and (3.18) and constraints mentioned in equation (3.22) are satisfied:

$$\begin{aligned} 0 \leq U(\gamma_i) \leq C_{max} 1.5V \leq V(\gamma_i) \leq V_{max} \\ 0.1\% \leq SoC(\gamma_i) \leq 100\% \end{aligned} \tag{3.22}$$

The first constraint limits the battery operation to a suitable value of input current upper and lower bounds. Other constraints are the physical limits of the battery. The value of V_{max} is $4.125V$ for the $CCCV$ algorithm. The value of C_{max} is between $1C$ and $4C$.

Equation (3.16) is a linear constraint of the NLP problem. Equation (3.18) is a nonlinear constraint of the NLP problem. The cost function of NLP is given by (3.21). Inequality constraints are mentioned in (3.22). The equations mentioned above constitute our NLP. The NLP is solved using MATLAB fmincon algorithm. To charge the Li-ion cell with less health degradation, the following cost function is adopted by the optimal controller:

$$\min_u J_c = \min_u \int_{t_0}^{t_f} \Big(Q_1 (SoC_{ref}(t) - SoC(t))^2 - Q_2 (J_s(t)) \Big) dt \tag{3.23}$$

We label the health-conscious controller as controller 1. Q_1 and Q_2 are weights to balance the charging speed and the degradation speed. The discretised cost function is given as follows:

$$\min_u J_c = \min_u \frac{t_f - t_0}{2} \Big[\sum_{i=0}^{i=P_H} Q_1 (SoC_{ref}(\gamma_i) - SoC(\gamma_i))^2 \alpha_i - Q_2 (J_s(\gamma_i)) \alpha_i \Big] \tag{3.24}$$

The second term in the cost function reduces health degradation. We have included J_s in the cost function as both health parameters, i.e. R_{film} and SoH are directly proportional to side reaction intercalation current J_s. SoC_{ref} is considered reference and provided in figure 3.2. We have preferred a ramp signal for $SoC_{ref}(t)$ over a constant SoC_{ref} as the input current designed by the optimisation algorithm is smoother. The slope of the ramp signal is equal to the maximum current. The specific value of slope implies that this is also a minimum time charging problem similar to the $CCCV$ charging case where we select $SoC_{ref}(t)$ as maximum SoC for minimum time charging.

Model Predictive Control

As the system model is nonlinear due to the nonlinear output voltage equation, we have used nonlinear model predictive control NMPC for optimal charging. At a particular time instant k, an NLP is formulated over P_H sampling instants up to time $k + P_H - 1$, and P_H samples of the input variable are calculated to minimise the NLP problem. In general, the number of the input samples (control horizon) is m, less than or equal to P_H. After a delay m samples, input is assumed constant up to prediction horizon P_H. In the present work, m and P_H are assumed to be equal. The following equation gives the optimal input vector:

$$\mathbf{u(k)} = [u(k|k), u(k+1|k), ...u(k+P_H-1|k)]^T \tag{3.25}$$

where $u(k + P_H - 1|k)$ is the input at time $k + P_H - 1$ predicted at time k using the system model.

Step No	Step
1	Available data: system model, initial conditions $x(0)$, prediction horizon P_H, control horizon $m = p$, parameters Q and R, constraint limits V_{min}, V_{max} etc
2	Solve the non-linear programming problem formulation 3.3.2 to obtain p samples of optimal input {u(1),u(2)...u(p).}
3	Use $u^* = u(1)$ to implement the controller.
4	Obtain the measured value of output y.
5	Estimate states x(we assume state feedback).
6	Update the initial conditions for the next iteration.
7	Repeat step 2 to step 6 for the next sampling instant.

Table 3.1: Non-linear model predictive control algorithm [11].

Only the first sample of optimal input vector $u(k|k)$ is implemented. The prediction process is repeated for each sampling instant online. The details of the algorithm are provided in table 3.1.

3.4 Results and Discussion

Control horizon m and prediction horizon P_H are set 3. A large value of m and P_H ensures better performance at the price of computational cost. Minimum values of the control and prediction horizon are selected for fast implementation of the algorithm. In our case, the optimisation algorithm showed a high value of errors for the control horizon and a prediction of less than three. The number of collocation points for the pseudo-spectral method is three, as the NLP can be solved in one iteration. I is the identity matrix. The sampling time is one seconds. NMPC is simulated using MATLAB fmincon algorithm.

Figure 3.1 shows the input current corresponding to the constraints $C_{max} = 2C$ on the input current. The input current for the $CCCV$ algorithm is maximum during the CC mode till 1600 seconds approximately for $2C$ input current upper bound. The input current decreases due to the maximum voltage constraint after the CC charging mode ends. We observe that the CV mode in the $CCCV$ charging algorithm over-penalises the input current. CV mode extends charging time for $CCCV$ charging algorithm. The controller 1 algorithm balances battery health and charging time efficiently. The $CCCV$ algorithm is not health-conscious and needs more charging time.

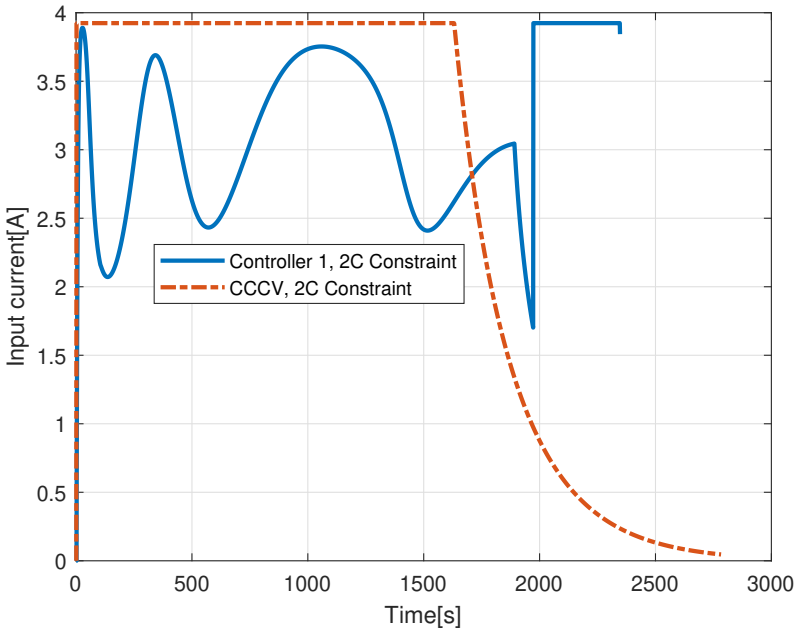

Figure 3.1: Comparison of the controller 1 and $CCCV$ charging algorithm for $2C$ input current upper bound. A comparison of the input current is shown.

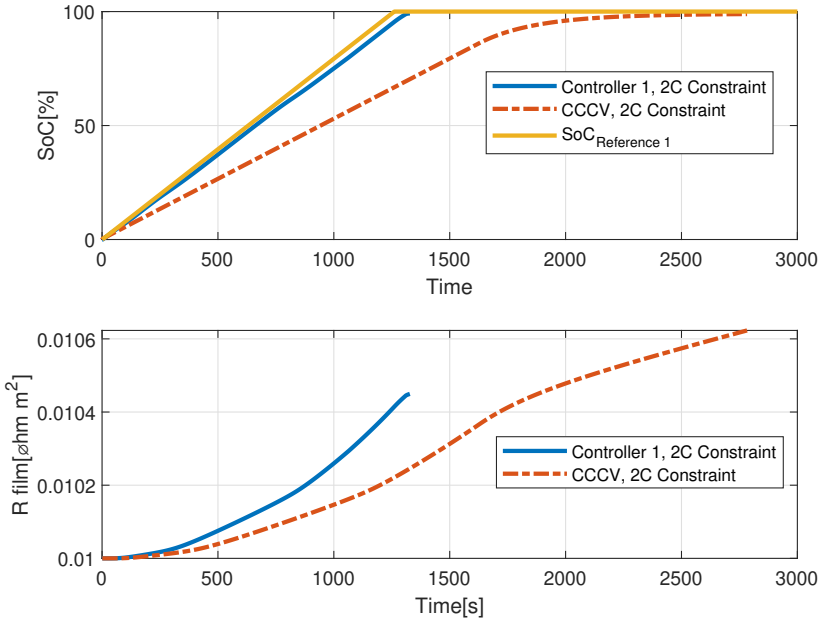

Figure 3.2: Comparison of the controller 1 and $CCCV$ charging strategies for $2C$ input current upper bound. Comparison of the SoC and Film resistance R_{film} is shown.

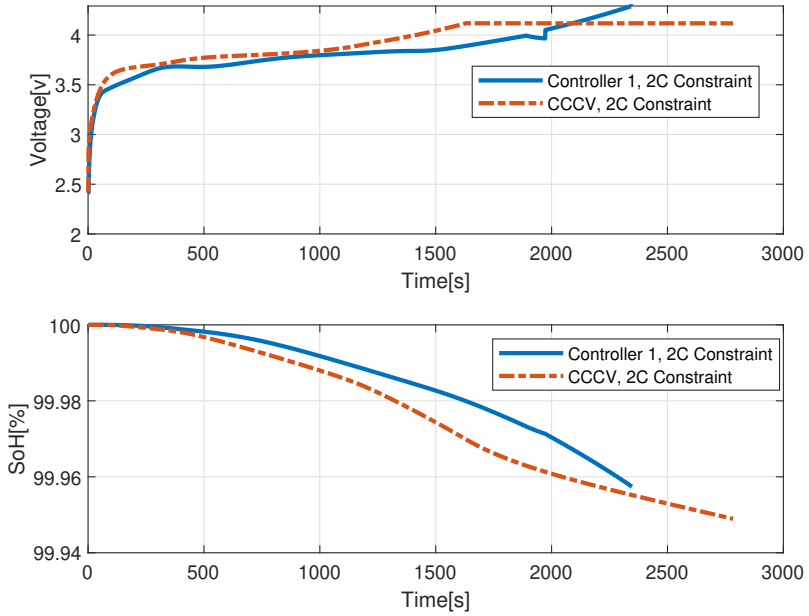

Figure 3.3: Comparison of the controller 1 and $CCCV$ charging strategies for $2C$ input current upper bound. A comparison of the output voltage and SoH is shown.

The algorithm execution time per iteration for the $CCCV$ charging algorithm and the controller 1 algorithm is $3ms$ and $19ms$, respectively. The $CCCV$ charging algorithm is faster than controller 1. However, the controller 1 algorithm is still computationally efficient, so real-time implementation of the algorithm is feasible. It is noteworthy that the simplified FHM model is more computationally efficient than state-of-the-art electrochemical models such as the simplified P2D model. So, a health-conscious charging algorithm based on the simplified FHM model will still be faster than the charging algorithm based on SPM. The algorithm execution time per iteration for the $CCCV$ charging algorithm based on the simplified FHM model and simplified P2D model is $3ms$ and $4ms$, respectively, as shown in table 3.2. The details of the simplified P2D model are given in [87].

Figure 3.2 shows R_{film} and SoC corresponding to constraints $C_{max} = 2C$ on the input current. The controller 1 charging increases R_{film} to 0.010494Ω while the $CCCV$ charging algorithm increases R_{film} to 0.01062Ω i.e. 1.2% more than the controller 1 charging algorithm. The SoC plot for the $CCCV$ charging has a high slope initially due to the CC charging mode and a low slope curve due to the CV charging mode. The

SoC plot for the controller 1 algorithm is relatively uniform.

Figure 3.3 shows the output voltage and SoH corresponding to constraints $C_{max} = 2C$. The controller 1 charging decreases SoH to 99.96% starting from 100% while the $CCCV$ charging algorithm decreases SoH to 99.95%. The controller 1 charging algorithm performed better according to all performance indicators of battery health while keeping the charging time slightly less. The difference between R_{film} and SoH becomes more significant for multiple cycles.

The effect of the input current upper bound C_{max} on the film resistance R_{film} and SoH for both algorithms is also studied. C_{max} is varied from $1C$ to $4C$, Whereas the value of $1C$ input current is $1.962A$. Figure 3.4a shows the effect of the input current upper bound on R_{film} at the end of a single cycle. R_{film} is large for small values of current upper bound C_{max}, but it gradually decreases and stabilises at a higher input current value. The SoH is defined based on capacity degradation. The SoH is minimum for $1C$ input current upper bound, and it gradually increases after $1C$ and stabilises at a higher value of input current upper bound as shown in Figure 3.4b. This pattern is opposite to the pattern observed in R_{film} plot. Many researchers have made similar observations [90].

Figure 3.5a, and figure 3.5b show the SoH and R_{film} plot for multiple cycles charging. Please note that the stoichiometric values, i.e. solid concentration corresponding to 0% and 100%, are updated at each cycle as mentioned in [60]. The input current constraint is $2C$. Although the difference in the SoH for the $CCCV$ charging and the controller 1 charging is small for a single cycle, the difference becomes substantial for multiple charging cycles. 80% SoH is generally considered the end of life for a Li-ion battery. We observe that the battery reaches 80% SoH after 392 cycles for $CCCV$ charging. At 392 cycles battery, SoH reaches 84.17% for the controller 1 charging. SoH reaches 80% after 484 cycles for the controller 1 charging. The battery life is extended by 92 cycles when charged with controller 1 charging. Significant performance improvement is possible due to controller 1 optimal charging. Similar behaviour is observed for R_{film}. After 392 cycles R_{film} value is 0.2032Ω and 0.2536Ω for the controller 1 algorithm and the $CCCV$ algorithm respectively. The $CCCV$ charging increases R_{film} by 24%. The

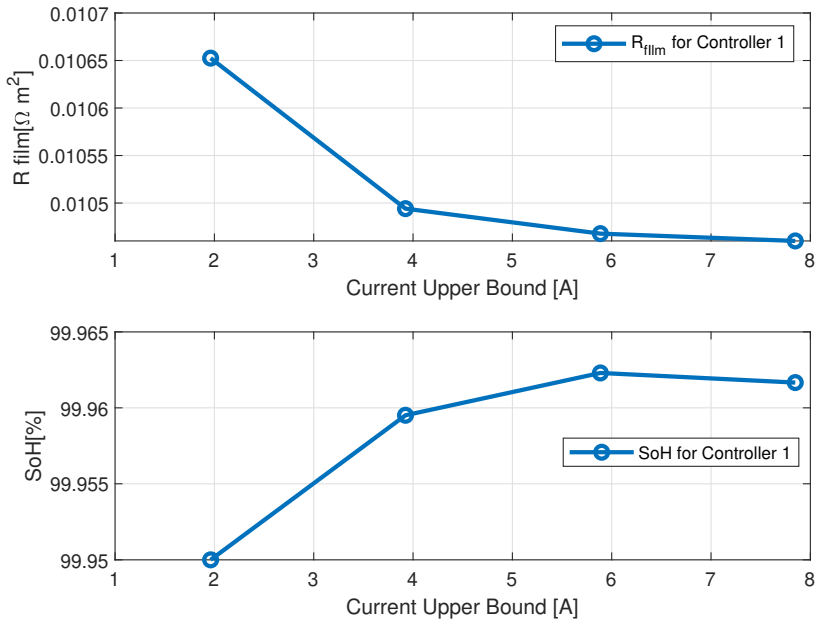

Figure 3.4: Analysis of the cell SoH. Figure (a) shows the film resistance R_{film} for the SFHM model using the controller 1 charging algorithm for various input current upper bound values at the end of a single cycle of charging. Figure (b) shows cell SoH for the SFHM model using the controller 1 charging algorithm for various input current upper bound values at the end of a single cycle of charging.

controller 1 charging algorithm reduces film resistance and health degradation more effectively than the $CCCV$ charging algorithm.

The effect of varying cost function weights Q_1 and Q_2 on controller performance is studied to tune the controller for optimal performance. Input current is constrained to $2C$. Q_2 is kept constant at 1×10^3 and Q_1 is varied. The input generated by the controller for various values of Q_1 is shown in figure 3.6. The SoC and SoH corresponding to the input in figure 3.6 are shown in figure 3.7. The value of Q_1 is varied from 2×10^1 to 4×10^3. The optimiser fails for Q_1 less than 2×10^1 and produces constant current input for values greater than 4×10^3. We observe that as we increase the cost function weight Q_1, the SoH performance improves. However, the SoC tracking is not good. Li-ion cell SoC equals SoC_{ref} for a maximum value of Q_1. It should be noted Q_1 and Q_2 are changed near full charging to tune the performance; however, these new values are unchanged for all simulations.

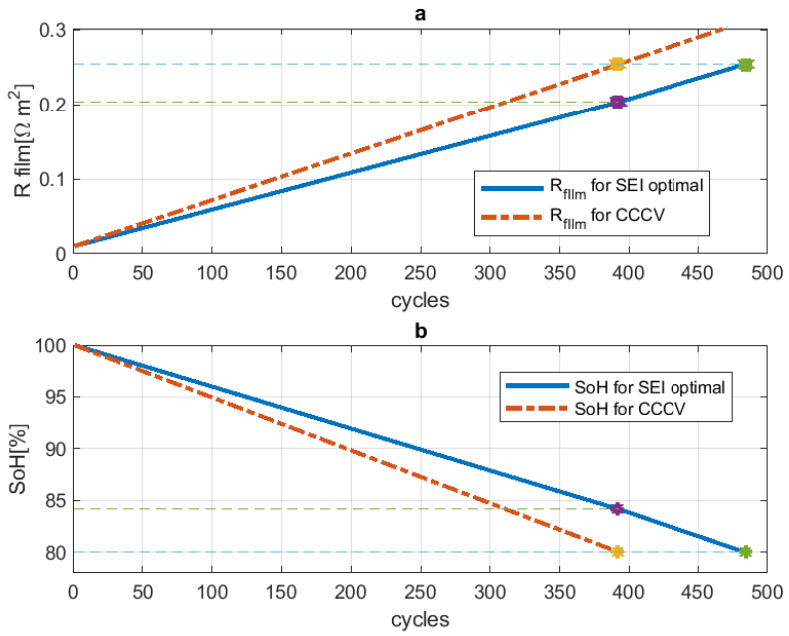

Figure 3.5: Analysis of the film resistance and the cell SoH for multiple cycle charging. Figure 3.5a shows the cell SoH for the SFHM model using the $CCCV$ charging algorithm and controller 1 charging algorithm. Figure 3.5b shows the film resistance (b) for the SFHM model using the $CCCV$ charging algorithm and controller 1 charging algorithm.

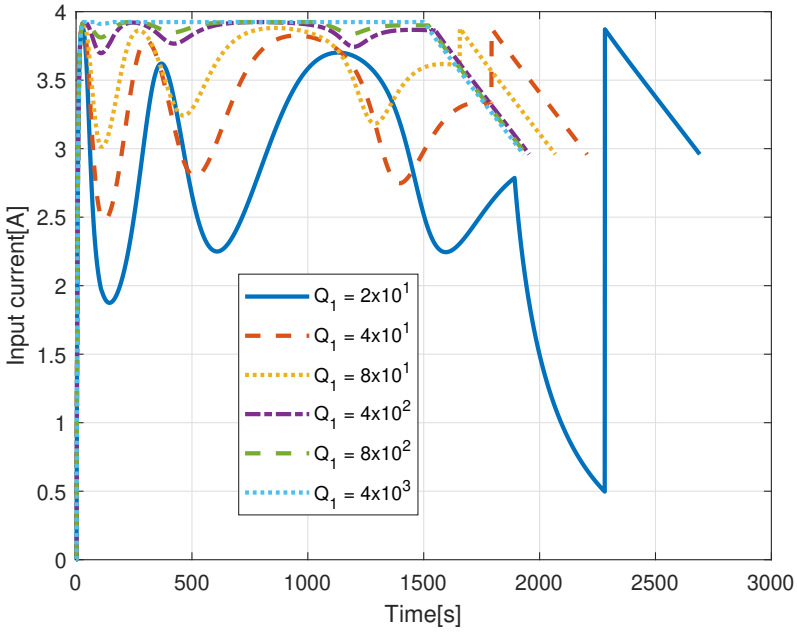

Figure 3.6: Current input for various values of weight Q_1 of cost function for $2C$ input current upper bound for controller 1.

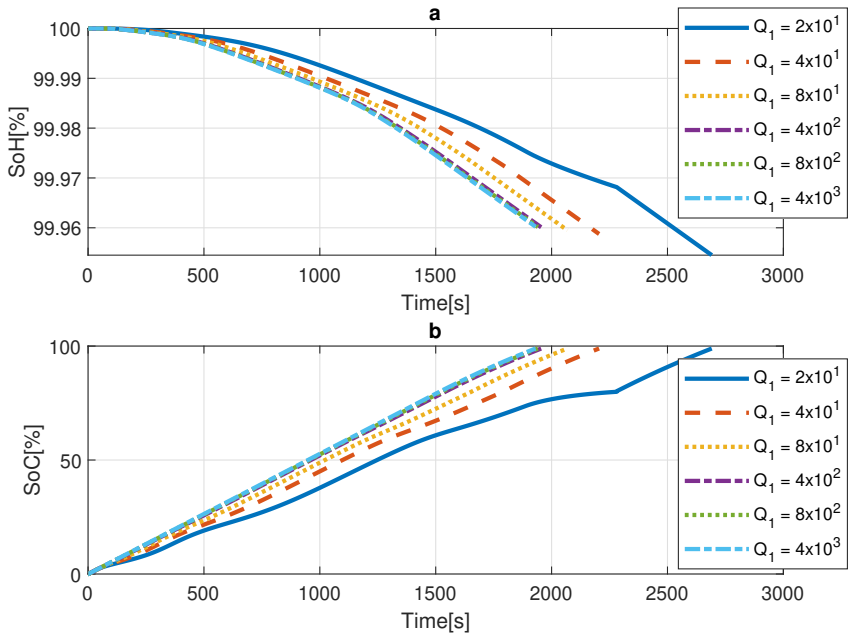

Figure 3.7: SoH and SoC for various values of weight Q_1 of cost function for $2C$ input current constraint for controller 1.

Algorithm	Algorithm execution time per iteration
$CCCV$ charging using SFHM model	$3ms$
$CCCV$ charging using SP2D model	$4ms$
Controller 1 charging using SFHM model	$19ms$

Table 3.2: Comparison of algorithm execution time for the Controller 1 charging algorithm based on the simplified FHM model and simplified P2D model for $2C$ input current upper bound.

Chapter 4

Output feedback optimal charging of a Li-ion cell

4.1 Introduction of SoC estimation

This chapter discusses output feedback charging of a Li-ion cell using several estimation algorithms. An estimator or observer improves the estimation accuracy if system signals are corrupted due to sensor noise or the system's parameters have slightly changed due to ageing or other reasons. The charging algorithm depends on the estimated states for closed-loop or output feedback charging. The performance of the charging algorithm based on output feedback will deteriorate further if an estimator is not used to minimise the effect of sensor noise and parameter uncertainties.

Numerous algorithms have been used to estimate SoC based on electrochemical and equivalent circuit models. A critical review of the models can be found in [65] and [16]. Extended Kalman filter (EKF), H infinity filter, recursive least square, sliding mode observer (SMO), least mean square, moving horizon estimator (MHE), and machine learning algorithms are a few examples of estimation methods that have been used to estimate Li-ion cell states. A comparative analysis of the algorithms can be found in the references mentioned above. As compared to conventional observers, moving horizon estimation has the additional benefit of systematically handling constraints while estimating system states at the cost of additional computation burden. MHE has been

used to estimate Li-ion cell dynamics using equivalent circuit models and electrochemical models [66], [67], [68], [69], [70], [71], [72], [73], [74], [75], [76].

Suthar *et al.* have implemented nonlinear MHE in an open loop for SoC estimation based on reformulated model. Although the feasibility of closed-loop charging using nonlinear MHE and nonlinear MPC is mentioned; however the simulation results of closed-loop charging are not provided [66]. Shen *et al.* have implemented nonlinear MHE in an open loop for SoC estimation based on an equivalent circuit model [74]. Zou *et al.* has implemented close loop control using MPC and MHE based on a linear model [91]. Zou *et al.* have also implemented nonlinear closed-loop control of a Li-ion cell using MPC, but the observer used is not MHE [92]. Rin *et al.* have used nonlinear MHE in an open loop for SoC estimation [71]. Shen *et al.* have implemented nonlinear joint MHE in an open loop for simultaneous parameter and SoC estimation. [67],[75]. Hu *et al.* have implemented a variant of MHE based on recursive least squares (RLS) called MH-RLS in an open loop for SoC estimation. [73]. Multi-time scale MHE is also presented to estimate SoH in addition to SoC estimation. Chen *et al.* have compared MHE and autoregressive long short-term memory (ARLSTM) and proved that a neural networks-based estimator is a good method to estimate SoC [76] when a system model is not available. Morabito *et al.* have presented a variant of MHE known as real-time iteration-based MHE (RTI-MHE) for real-time SoC estimation, which makes it useful for practical BMS applications [68]. Liu *et al.* have presented a computationally efficient MH approach for total least squares (TLS) SoC estimation [70], which is more accurate than the unscented Kalman filter. The algorithm is more efficient than a simple MHE algorithm due to the use of a differential flatness algorithm.

None of the earlier references has implemented optimal charging in a closed loop using a nonlinear MPC and nonlinear MHE based on an electrochemical model.

4.1.1 Novelty

The literature review suggests that a simplified FHM model is not used to estimate Li-ion cell's SoC/SoH till now. The simplified FHM model is computationally efficient and more accurate than SPM [87]. Estimators' computational efficiency and accuracy

based on a simplified FHM model will also be higher than estimation based on an SPM. The novel contribution of this work is the SoC or SoH estimation of a Li-ion cell based on a simplified FHM model.

As the simplified FHM model is recently developed, No literature about its observability is available. Another novelty of this article is the observability analysis of the simplified FHM model. A thorough study of observability and comparison of the simplified FHM model with SPM reveals that, similar to the SPM model, the simplified FHM model is weakly observable. Weak observability implies a deterioration in estimation accuracy. The output voltage depends on the difference between the open-circuit potentials of the anode and cathode. As the output voltage does not depend on the Li-ion concentration in the individual electrodes, the estimation of Li-ion concentration in individual electrodes based on only voltage measurement is inaccurate. Studies show that the observability matrix of the SPM is full rank, i.e. the model is observable. However, the condition number of the observability matrix is high. A high condition number implies weak observability, i.e. the estimation accuracy is not good [93]. An equal percentage of SoC is assumed in the anode and cathode, and the SoC of only one electrode is estimated to resolve this problem,[94], [95], [96]. Our work is also based on the same principle.

Although there have been many closed-loop charging attempts, the attempts are either based on a linear MPC and MHE or a nonlinear MPC based on estimation algorithms other than MHE. MHE can handle constraints systematically, unlike other estimators, and its problem formulation is similar to MPC. Another novelty of the paper is using a nonlinear MPC and a nonlinear MHE for closed-loop charging. The performance of the MHE algorithm is compared with SMO and EKF in open and closed loops in the presence of zero-mean additive white Gaussian noise and parameter perturbation in the system.

The SEI layer model mentioned in [56], [63], and [57] is included in the simplified FHM model for health-conscious charging. Orthogonal collocation is used to convert the optimal control problem (OCP) or optimal estimation problem to a nonlinear pro-

gramming problem (NLP) to increase the computational efficiency of the algorithm. Li-ion liquid concentration estimation is implemented in an open loop to enhance the computational efficiency of estimation. The stability of open loop estimation is discussed in the literature [97].

This chapter is organised as follows. Extended Kalman filter (EKF), sliding mode observer (SMO) and moving horizon estimator (MHE) is discussed in section 4.1.2, 4.1.3 and 4.2, respectively. Section 4.3 presents results, analysis and discussion.

4.1.2 Extended Kalman filter

Extended Kalman filter (EKF) and its application to *SoC* estimation are studied and analysed in great depth. EKF has been used to estimate *SoC* using both equivalent circuit models, such as the work of Plet *et al.* [12],[13], and electrochemical models, such as the work of Tanim *et al.* and Tran *et al.* [26], [98]. Here is a brief review of the algorithm to facilitate the reader.

The mathematical model of a Li-ion cell is nonlinear due to non-linearity in the output voltage equation. The state space model of a nonlinear system is given as follows.

$$x_{k+1} = f(x_k, u_k) + w_k \tag{4.1}$$

$$y_k = g(x_k) + v_k \tag{4.2}$$

x represents system states. Li-ion concentration in the electrode is the only state of the system as liquid concentration is estimated in an open loop. u is a system input variable, i.e. input current of a Li-ion cell. f is the state function of a Li-ion cell, i.e. solid diffusion equation. g is an output function of Li-ion cell, i.e. the voltage equation 2.43 and *SoC* equation 3.14. Other variables of a Li-ion cell, such as over potential, exchange current density, solid and liquid potential, are considered part of the output equation. Intercalation current is considered part of the input equation as it is directly proportional to the input current. w_k and v_k are process noise and measurement noise variables. The state-space model of time-invariant linear or linearised systems is as

follows.

$$x_{k+1} = A_s x_k + B_s u_k + w_k \tag{4.3}$$

$$y_k = C_s x_k + v_k \tag{4.4}$$

The state matrix A_s, input matrix B_s and output matrix C_s are obtained by linearisation of state function f and output function g as mentioned in the following equations.

$$A_s = \frac{\partial f(x_k, u_k)}{\partial x_k}$$

$$B_s = \frac{\partial f(x_k, u_k)}{\partial u_k}$$

$$C_s = \frac{\partial g(x_k, u_k)}{\partial x_k}$$

The matrices are calculated offline and stored. In this case, the state equation is already linear. So we don't have to perform linearisation for state equation and matrices A and B are readily available. Firstly, the system states and error covariance of states are predicted using the system model and error statistics, as mentioned next:

$$\hat{x}_{k+1|k} = f(x_k|k, u_k) + w_k$$

$$P_{k+1|k} = A_s P_{k|k} A_s^T + Q_{k+1}$$

This is called the prediction step or time update. The error covariance provides information about the uncertainty of system state estimation. Next, the state and error covariance predictions are updated based on the sensor measurement of the output signal, i.e. the output voltage equation of a Li-ion cell. The step is called the correction step or measurement update.

$$\tilde{y}_{k+1} = y_{k+1} - g(\hat{x}_{k+1|k})$$

$$\boldsymbol{K}_{k+1} = P_{k+1|k} C_s^{'} (C_s P_{k+1|k} C_s^{'} + R_{k+1})^{-1}$$

$$x_{k+1|k+1} = \hat{x}_{k+1|k} + \boldsymbol{K}_{k+1} \tilde{y}_{k+1}$$

$$P_{k+1|k+1} = P_{k+1|k} - \boldsymbol{K}_{k+1} C_s^{'} P_{k+1|k}$$

$\hat{x}_{k|k}$ and $\hat{x}_{k+1|k}$ are the *a priori* and *a posteriori* state estimates respectively. $P_{k|k}$ and $P_{k+1|k}$ are the *a priori* and *a posteriori* covariance matrix respectively. Q and R are the covariances of process noise and measurement noise, respectively the value of these covariances are given in the results section. The symbol $'$ is used for transpose. $\tilde{y}$ is the output estimation error. The output estimation error is dependent on the accuracy of the model. If the time update is accurate, the measurement update will make less change in estimated values.

$\boldsymbol{K}$ is the Kalman gain designed to minimise the mean square error. The initial value of error covariance is assumed to be zero. While the initial state of the system is given by the initial concentration of Li-ion in the electrode. The initial concentration of Li-ion in the electrolyte is equal to the average concentration, as it is reasonable to assume that the cell is at rest for a considerably long time.

As discussed earlier, Li-ion concentration in electrolytes is estimated in an open loop. The remaining simulation details are discussed in the Results section 4.3. Please note that the Li-ion concentration in the electrolyte is estimated in an open loop. In contrast, the estimation of solid concentration is done for only one electrode, and the solid concentration in the other electrode is assumed to be equivalent to the first electrode. 4.3. Table 4.1 shows the detailed procedure of the EKF algorithm along with an MPC controller in a closed loop.

4.1.3 Sliding mode observer

An EKF is based on a linearised model; hence, it is not a true nonlinear estimator. A sliding mode observer (SMO) is a nonlinear estimator that incorporates the system's nonlinear model to estimate system states. Some researchers have observed that EKF is relatively less sensitive to noise in output measurement. In comparison, SMO shows superior performance in the presence of input disturbance or parameter perturbation [99]. SMO has been used to estimate Li-ion cell SoC using the equivalent circuit and electrochemical models [96], [100].

Here only a brief review of the observer is presented. The following equations describe a

Step No	Step
	Available data: linearised system model i.e. matrices A, B and C, prediction horizon for controller MPC p_1,
1	Initial state of the system i.e. solid concentration x^*, control horizon $m = p_2$, process noise and measurement noise variance Q and R, constraints of the system
2	Use $x^* = x(k)$ as initial condition.
3	Using the initial condition, solve the non-linear programming problem formulation 3.3.2 to obtain p samples of optimal input $\{u(1), u(2)...u(p_2).\}$
4	Use $u^* = u(1)$ to implement the controller.
5	Obtain the measured value of output y.
6	Based on prediction step or time update equation of EKF, to estimate Li-ion output voltage using table 2.5, table 2.6 and equation 2.43.
7	Calculate estimation error using measured output voltage and predicted output voltage.
8	Based on estimation error, Use correction step or measurement update equation of EKF to obtain the correct value of estimate Li-ion output voltage.
9	The estimated states are the current states of system x^*.
10	Repeat step 2 to step 9 for the next sampling instant.

Table 4.1: Non-linear MPC charging algorithm based on EKF [11].

Li-ion cell model.

$$\dot{x}(t) = Ax + Bu + w$$

$$y = g(x, u) + v$$

The first equation is the state equation of a Li-ion cell, i.e. diffusion equation of electrode as mentioned in table 2.5, which is linear. Li-ion concentration in the anode is the only state of the system. The second equation is the output equation, i.e. voltage equation 2.43, which is nonlinear. Other algebraic equations of a Li-ion cell, such as over potential equation 2.40 and exchange current density equation, are considered part of the output equation. w is process noise and v is measurement noise. An SMO is designed by considering the estimation error as the sliding surface.

$$\dot{\hat{x}}(t) = A\hat{x} + Bu + Msign(\tilde{x}) \tag{4.5}$$

$$\hat{y} = g(\hat{x}, u) \tag{4.6}$$

$$\tilde{x} = x - \hat{x}$$

$\dot{\hat{x}}(t)$ is the estimate of Li-ion cell state, i.e. Li-ion concentration in the electrode as liquid concentration is estimated in an open loop. $\tilde{x}$ is estimation error.

The Lyapunov analysis is used to calculate the value of observer gain M. As mentioned below, the square of estimation error is considered the Lyapunov function.

$$V = 0.5\tilde{x}^2$$

$$\dot{V} = \tilde{x}\dot{\tilde{x}}$$

$$\dot{V} = \tilde{x}(\dot{x} - \dot{\hat{x}})$$

$$\dot{V} = \tilde{x}[Ax + Bu - (A\hat{x} + Bu + Msign(\tilde{x}))]$$

$$\dot{V} = \tilde{x}[Ax - A\hat{x} + Bu - Bu - Msign(\tilde{x}))]$$

$$\dot{V} = \tilde{x}[A\tilde{x} - Msign(\tilde{x}))]$$

According to Lyapunov theory, a derivative of the Lyapunov function must be negative for a stable system. To obtain $\dot{V} < 0$, A suitable value of parameter M is required.

$$\tilde{x}[A\tilde{x} - Msign(\tilde{x}))] < 0$$

$$M > \frac{\tilde{x}A\tilde{x}}{|\tilde{x}|}$$

$$M > A|\tilde{x}|$$

To find a suitable value of M, let us assume, in a worst-case scenario, i.e. the maximum error is equal to the maximum value of Li-ion concentration in the electrode when the estimated value is zero. The maximum and minimum Li-ion concentration in an electrode is known. A suitable value of the coefficient M can satisfy the equation.

Please note that the assumptions made previously are still valid, i.e. open loop estimation of Li-ion concentration in electrolyte and estimation of solid concentration for only one electrode. As M is the only parameter of the sliding mode observer, the design of a basic sliding mode observer is simpler than other observers.

Step No	Step
	Available data: linearised system model, i.e. matrices A, B and C, prediction horizon for controller MPC p_1,
1	Initial state of the system, i.e. solid concentration x^*, control horizon $m = p_2$, process noise and measurement noise variance Q and R, constraints of the system
2	Use $x^* = x(k)$ as initial condition.
3	Using the initial condition, solve the non-linear programming problem formulation 3.3.2 to obtain p samples of optimal input $\{u(1), u(2)...u(p_2).\}$
4	Use $u^* = u(1)$ to implement the controller.
5	Obtain the measured value of output y.
6	Based on SMO state equation 4.5 and output equation 4.6, estimate Li-ion output voltage.
7	The estimated states are the current states of the system x^*.
8	Repeat step 2 to step 7 for the next sampling instant.

Table 4.2: Non-linear MPC charging algorithm based on SMO [11].

The details of noise and perturbation analysis are discussed in the results section 4.3. Table 4.1 shows the detailed procedure of the SMO algorithm along with an MPC controller in a closed loop.

4.2 Moving horizon estimation

Estimation algorithms such as EKF and SMO can not handle constraints, whereas moving horizon estimation (MHE) is suitable to handle constraints. The formulation of MHE using probability theory is briefly discussed in this work. The detailed proof is mentioned in [101]).

Let us assume x_k represents the states of the system and y_k represents the system's output. Let us assume that at a particular time instant $T_1 - 1$, the system's output is available for $k = 0...T_1 - 1$. We want to know the value of system states during this period. Let us assume system states and output are corrupted by process noise w_k and sensor noise v_k, respectively. The problem statement is expressed using maximum *a posteriori* Bayesian estimate as mentioned below.

$$\begin{aligned} \{\hat{x}_{0|T_1-1}, \hat{x}_{1|T_1-1}, \hat{x}_{2|T_1-1}..., \hat{x}_{T_1|T_1-1}\} = \\ arg \max_{x_0, x_1, x_2...x_{T_1-1}} p(x_0, x_1, x_2...x_{T_1}|y_0, y_1..y_{T_1-1}) \end{aligned} \tag{4.7}$$

The following equation represents state space formulation-based systems.

$$x_{k+1} = f(x_k, u_k) + w_k \tag{4.8}$$

$$y_k = g(x_k, u_k) + v_k \tag{4.9}$$

The following equation gives the estimation problem mentioned in the equation 4.7 for state space systems. [102].

$$\max_{x_0, x_1, x_2 ... x_{T_1} - 1} p(x_0, x_1, x_2 ... x_{T_1} | y_0, y_1 .. y_{T_1 - 1}) = \min_{x_0, \{w\}_{k=0}^{T_1 - 1}} \phi_{T_1}(x_0, \{w_k\}) \tag{4.10}$$

$$\phi_{T_1}(x_0, \{w_k\}_{k=0}^{T_1-1}) = \sum_{k=0}^{T_1-1} ||v_k|| R_{1,k}^{-1} + ||w_k|| R_{2,k}^{-1} + ||x_0 - \hat{x}_0|| R_{3,k}^{-1} \tag{4.11}$$

$\hat{x}_0$ is *a priori* estimate of initial conditions. The first and second terms in the equation minimise the effect of measurement noise and process noise, respectively, whereas the last term minimises the error of the initial state estimate. Given past T_1 samples of output, our goal is to find the value of system states for past m time instants, which maximises the conditional probability. The equation implies that maximising the conditional *a priori* probability for state space systems is equivalent to minimising the effect measurement noise, process noise and estimation error of initial conditions. Online implementation of the **full information problem** becomes infeasible as the data size increases. Let us assume that the estimator can process only p_1 samples (prediction horizon) per iteration.

$$\phi_{T_1}(x_0, \{w_k\}_{k=0}^{T_1-1}) = \sum_{k=T_1-p_1}^{T_1-1} ||v_k|| R_{1,k}^{-1} + ||w_k|| R_{2,k}^{-1} + ||x_0 - \hat{x}_0|| R_{3,k}^{-1} + Z_{T_1-p_1} \tag{4.12}$$

$$Z_{T_1-p_1} = \sum_{k=0}^{T_1-p_1-1} ||v_k|| R_{1,k}^{-1} + ||w_k|| R_{2,k}^{-1} + ||x_0 - \hat{x}_0|| R_{3,k}^{-1} \tag{4.13}$$

The arrival cost $Z_{T_1-p_1}$ approximates the effect of the samples outside the prediction horizon. The most straightforward approach is to assume zero arrival cost. We have only considered minimising v_k, and a simple optimisation problem for SoC estimation

of a Li-ion cell is used.

$$\max_{x_0,x_1,x_2...x_{T_1}-1} p(x_0,x_1,x_2...x_{T_1}|y_0,y_1..y_{T_1-1}) = \min_{x_0,\{w\}_{k=0}^{T_1-1}} \sum_{k=T_1-N_1}^{T_1-1} ||y_k - h(x_k,u_k)||R_{1,k}^{-1} \tag{4.14}$$

The pseudo-spectral formulation of the nonlinear programming problem is mentioned as follows.

$$\max_{x_0,x_1,x_2...x_{T_1-1}} p(x_0,x_1,x_2...x_{T_1}|y_0,y_1..y_{T_1-1}) = \min_{x_0,\{w\}_{k=0}^{T_1-1}} \frac{t_f - t_0}{2} \sum_{k=T_1-p_1}^{T_1-1} ||Y(\gamma_k) - H(X(\gamma_k),U(\gamma_k))\alpha_k||R_{1,k}^{-1} \tag{4.15}$$

γ_i is the collocation point or discretised time.

4.2.1 Non-linear programming problem formulation

Average solid concentration in electrodes $\bar{c_n}(t)$ and $\bar{c_p}(t)$ and total liquid concentration in electrolyte $Q_{e,n}$, $Q_{e,s}$ $Q_{e,p}$ are states of the non-linear state space model (i.e. simplified FHM model) of Li-ion cell. Equations (2.23), (2.36), (2.37) and (2.38) are dynamic equations of the simplified model as the time derivative of states is given by these equations. The equations can be grouped and represented as follows:

$$\dot{x}(t) = f(x(t),u(t)) \tag{4.16}$$

Output equation (2.43) is an algebraic equation and is represented as follows.

$$y = g(x,u) \tag{4.17}$$

f, x, u, y and g are state functions, system state, input, output variables, and output functions, respectively. Solid and liquid concentration variables are considered the state variables of a cell.

The equation is discretised using orthogonal collocation. The details of orthogonal collocation are discussed in section 2.4. The N dimensional matrix equation corresponding

to N collocation points is expressed as follows:

$$X_{N\times 1} = X(t_0)_{N\times 1} + \frac{t_f - t_0}{2} A_{N\times N} F_{N\times 1}(X, U) \tag{4.18}$$

$A_{N\times N}$ is the integration matrix. Value of state matrix G is given as follows:

$$F = \begin{bmatrix} -\frac{J(x_N)}{3\eta_s \cdot F} - \frac{I_{app}}{F \cdot L_n} \\ -\frac{J(x_N)}{3\eta_s \cdot F} - \frac{I_{app}}{F \cdot L_p} \\ \frac{I_{app}(1-t_+)}{F} + D_{e,n} 2a_1 L_n \\ -\frac{I_{app}(1-t_+)}{F} + D_{e,p} 2a_6 L_p \\ D_{e,s} 2a_4 L_s \end{bmatrix} \tag{4.19}$$

The output equation (2.43) is an algebraic equation. The following equation represents the output equation in matrix form:

$$Y_{N\times 1} = G_{N\times 1}(X, U) \tag{4.20}$$

The output matrix G for voltage output Y is as follows.

$$G = \bar{\eta_p}(\gamma_i) - \bar{\eta_n}(\gamma_i) + U_{c,p}(\theta(\gamma_N)) - U_{c,n}(\theta(\gamma_0)) + k_1 I_{app} + k_2(\ln(C_{e,p}(\gamma_N)) - \ln(C_{e,n}(\gamma_0))) \tag{4.21}$$

γ_i is the collocation point or discretised time.

The optimisation problem is to find the value of initial states for past p_1 samples to minimise a cost function J such that system equations (4.18) and (4.20) and constraints mentioned in the equation 4.23 are satisfied for provided samples of input u and output y:

The cost function is mentioned below:

$$\underset{x_0}{min} J = \min_{x_0, \{w\}_{k=0}^{T_1-1}} \frac{t_f - t_0}{2} \sum_{k=T_1-p_1}^{T_1-1} ||Y(\gamma_k) - H(X(\gamma_i), U(\gamma_i))\alpha_k||R_{1,k}^{-1} \tag{4.22}$$

Step No	Step
1	Available data: system model, prediction horizon for controller p_2, prediction horizon for observer p_1, Past p_1 samples of output, control horizon $m = p_2$, parameters Q and R, constraints of the system
2	Solve the non-linear programming problem formulation 4.15 to obtain p samples of system states $\{x(k-p_1), x(k-p_1+1)...x(k).\}$
3	Use $x^* = x(k)$ as initial condition.
4	Using the initial condition, solve the non-linear programming problem formulation 3.3.2 to obtain p samples of optimal input $\{u(1), u(2)...u(p_2).\}$
5	Use $u^* = u(1)$ to implement the controller.
6	Obtain the measured value of the output y.
7	Repeat step 2 to step 6 for the next sampling instant.

Table 4.3: Non-linear MPC charging algorithm based on MHE [11].

The system operation is constrained by the limits mentioned in the following equations:

$$\begin{aligned} 0 \leq U(\gamma_i) \leq C_{max} \\ 1.5V \leq V(\gamma_i) \leq V_{max} \\ 0.1\% \leq SoC(\gamma_i) \leq 100\% \end{aligned} \tag{4.23}$$

The first constraint limits the battery operation to a suitable input current value. Other constraints are the physical limits of the battery. The value of V_{max} is $4.125V$ for the $CCCV$ algorithm. The value of C_{max} is between $1C$ and $4C$.

System equation (4.18) is a linear constraint of the NLP problem. Output equation (4.20) is a non-linear constraint of the NLP problem. The equation (4.22) gives the cost function of NLP. Inequality constraints are mentioned in the equation (4.23). The equations mentioned above constitute our NLP. The NLP is solved using MATLAB fmincon algorithm to obtain the following result.

$$\mathbf{x\_e} = [x(k-p_1), x(k-p_1+1), ...x(k-1), x(k)]^T \tag{4.24}$$

$x(k+p_1-1|k)$ is the initial state at time instant $k+p_1-1$ predicted at time k using the system model.

The last initial state vector $x(k)$ sample is used as an initial state value. The prediction process is repeated for each sampling instant online. The details of the algorithm are provided in Table 4.3.

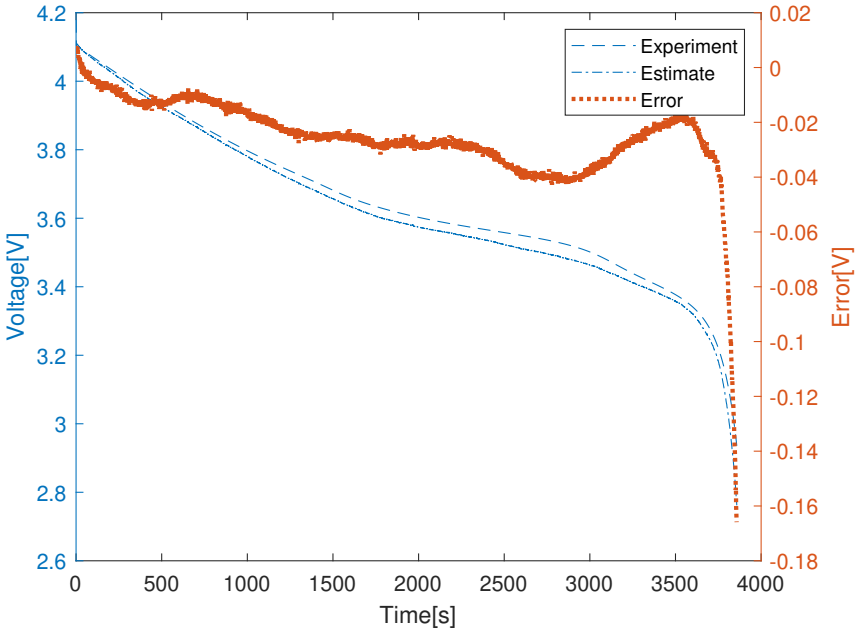

Figure 4.1: The output voltage of a Li-ion cell estimated by EKF for $1C$ input current. 1mV variance noise is added to the experimental voltage. [6].

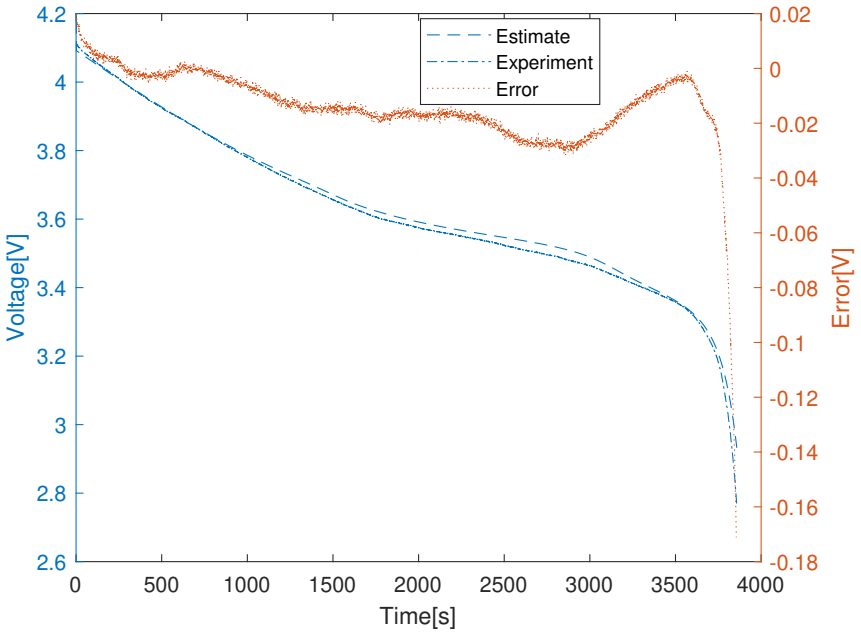

Figure 4.2: The output voltage of a Li-ion cell estimated by SMO for $1C$ input current. 1mV variance noise is added to the experimental voltage. [6].

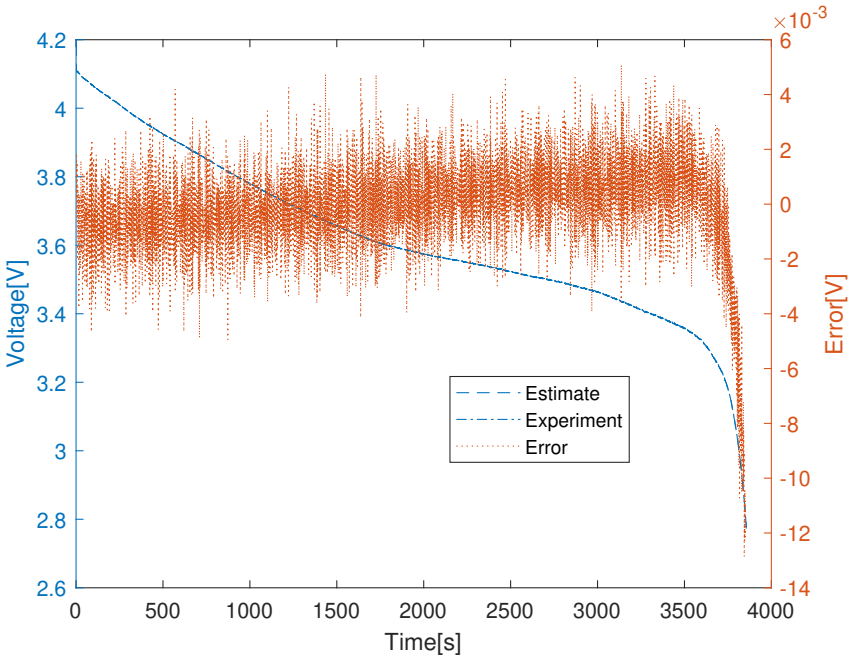

Figure 4.3: The output voltage of a Li-ion cell estimated by MHE for $1C$ input current. 1mV variance noise is added to the experimental voltage. [6].

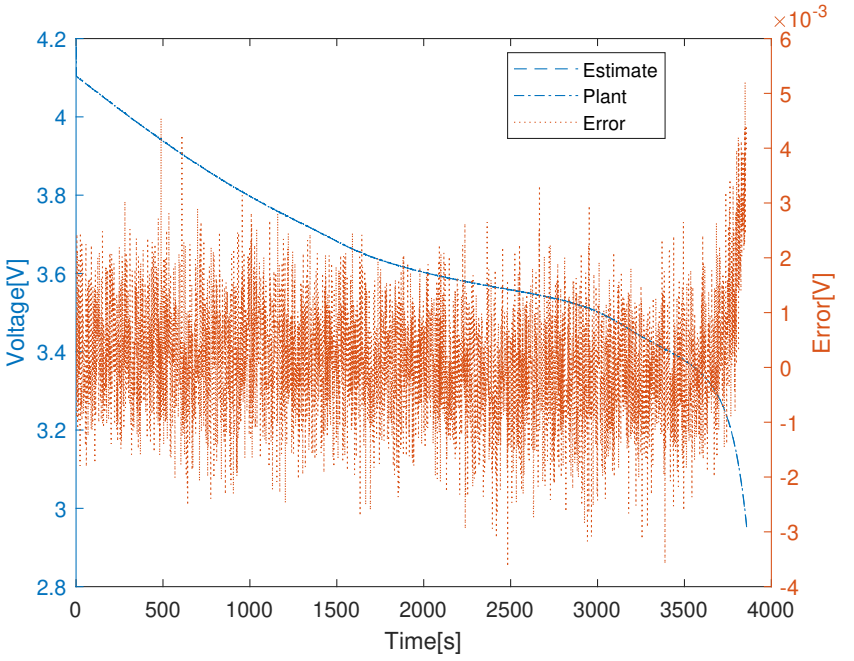

Figure 4.4: The output voltage of a Li-ion cell estimated by EKF for $1C$ input current. 1mV variance noise is added to the plant output voltage.

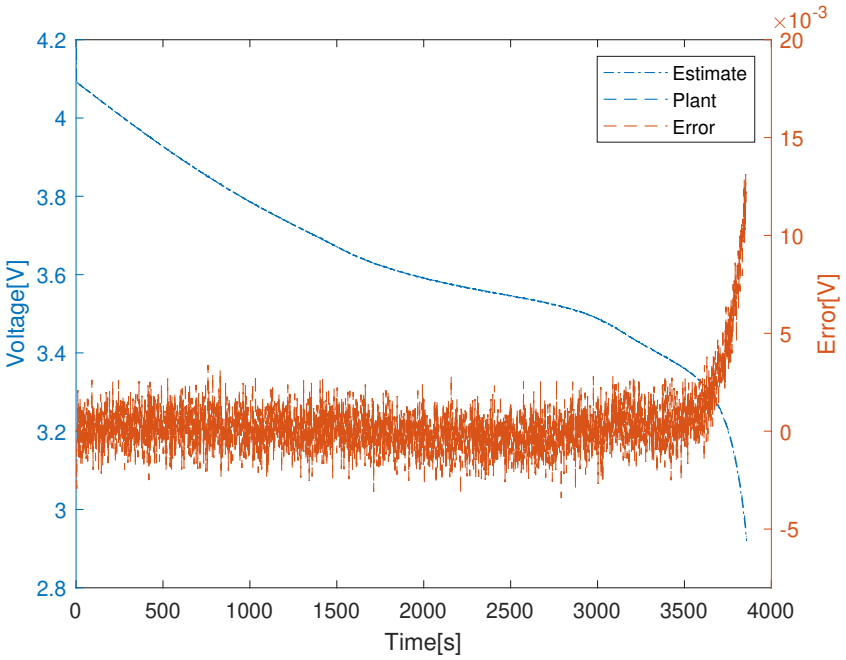

Figure 4.5: The output voltage of a Li-ion cell estimated by SMO for $1C$ input current. 1mV variance noise is added to the plant output voltage.

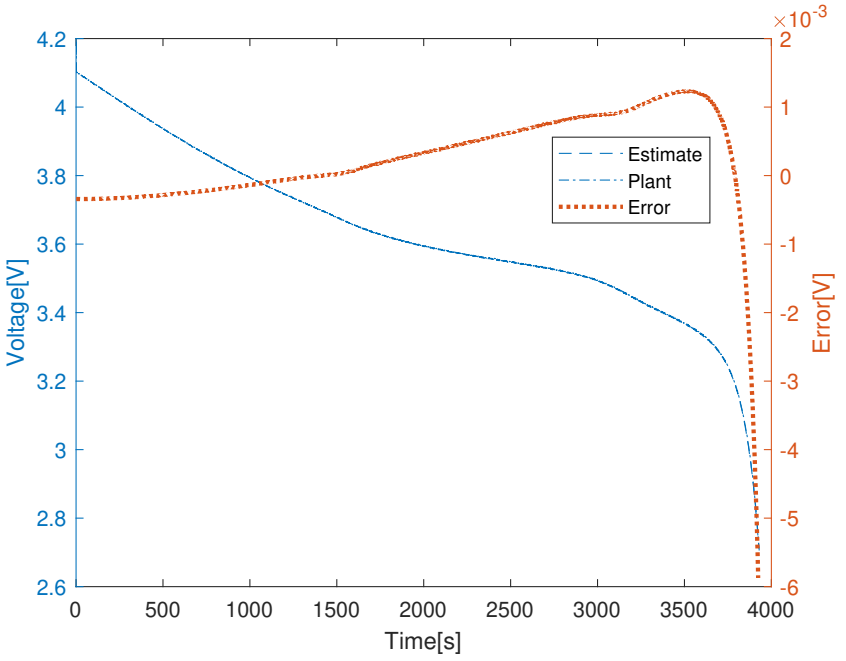

Figure 4.6: The output voltage of a Li-ion cell estimated by MHE for $1C$ input current. 1mV variance noise is added to the plant output voltage.

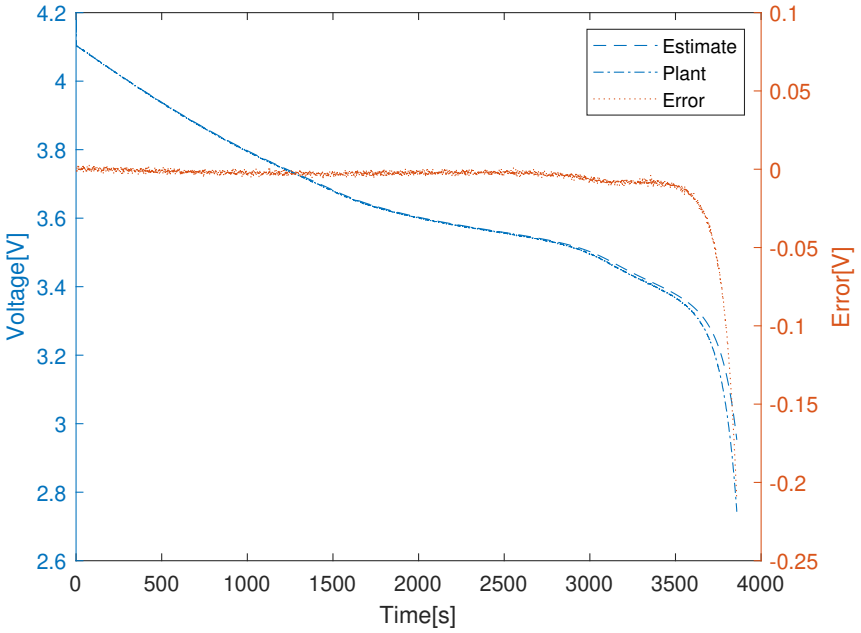

Figure 4.7: The output voltage of a Li-ion cell estimated by EKF for $1C$ input current in the presence of 1mv variance voltage and diffusion equation parameters perturbed by 1%.

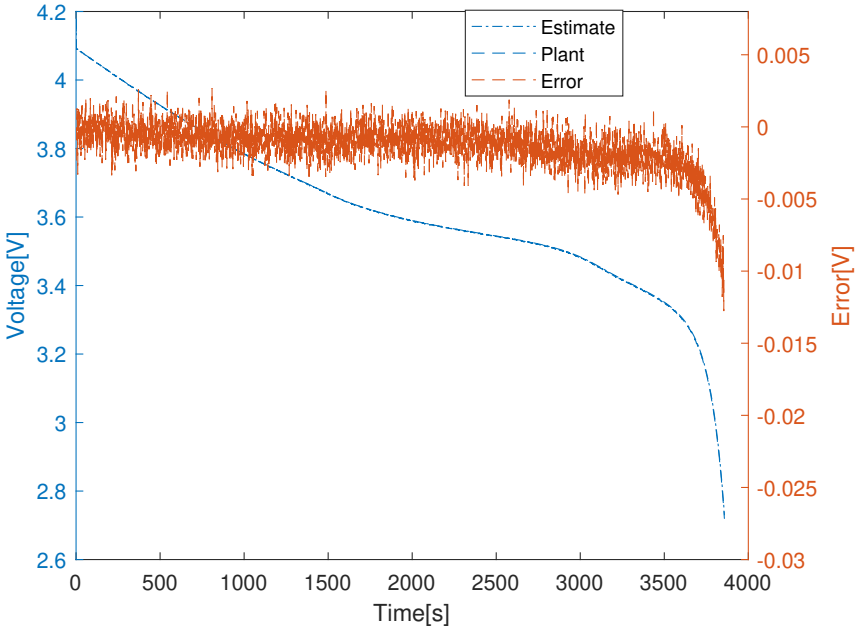

Figure 4.8: The output voltage of a Li-ion cell estimated by SMO for $1C$ input current in the presence of 1mV variance voltage and diffusion equation parameters perturbed by 1%.

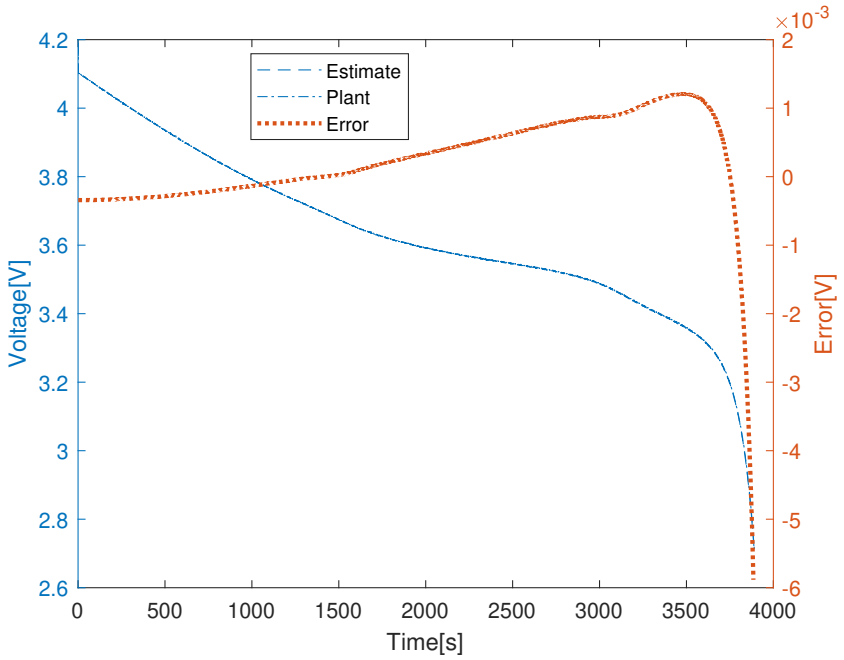

Figure 4.9: The output voltage of a Li-ion cell estimated by MHE for $1C$ input current in the presence of 1mV variance voltage and diffusion equation parameters perturbed by 1%.

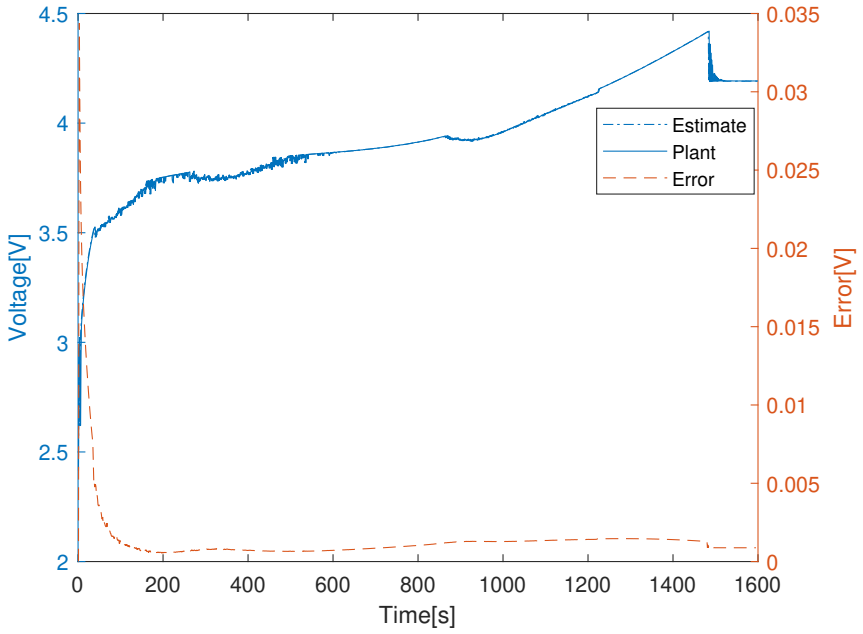

Figure 4.10: The output voltage of a Li-ion cell estimated by MHE for optimal input current designed using model predictive control 0.2mV variance noise is added to the plant output voltage.

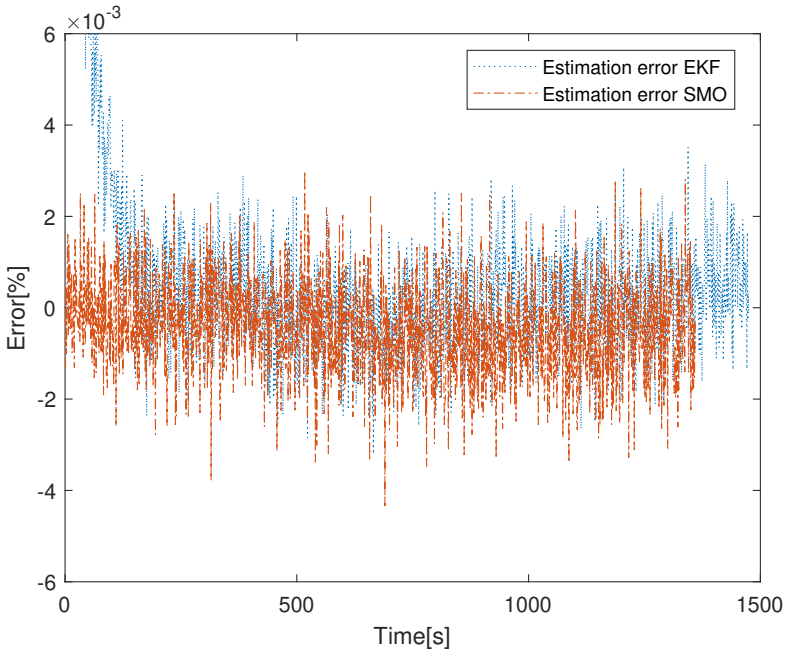

Figure 4.11: The output voltage estimation error of a Li-ion cell estimated by EKF and SMO for optimal input current designed using the model predictive control. 0.2mV variance noise is added to the plant output voltage.

Algorithm	Algorithm execution time per iteration	Open loop RMSE
EKF	$0.0003s$	0.83%
SMO	$0.0003s$	0.59%
MHE	$0.007s$	0.06%

Table 4.4: Comparison of Algorithm execution time and RMS error for various estimation algorithms in open loop configuration for $1C$ current at 318K temperature. Experimental voltage is considered a reference.

Algorithm	RMSE for 1mv Noise	Error variance	RMSE for 1mv Noise and 1 % perturbation	Error variance
EKF	0.03%	$20\mu V$	0.2%	$40\mu V$
SMO	0.04%	$1\mu V$	0.05%	$16\mu V$
MHE	0.04%	$12\mu V$	0.05%	$12\mu V$

Table 4.5: Comparison of RMS error for various estimation algorithms in open loop configuration for $1C$ current at 318K temperature. Only solid diffusion equation is perturbed by 1%. The simulated plant output voltage is considered a reference.

Algorithm	Root mean square error RMSE	Error variance
EKF	0.35%	$50\mu V$
SMO	0.15%	$17\mu V$
MHE	0.09%	$12\mu V$

Table 4.6: Comparison of RMS error for various estimation algorithms in open loop configuration for $1C$ current at 318K temperature. All parameters of the Li-ion cell model are perturbed by 1%. The simulated plant output voltage is considered a reference.

Algorithm	Algorithm execution time per iteration	Closed loop RMSE	Error variance
EKF	$0.007s$	3%	$50\mu V$
SMO	$0.009s$	3.6%	$10\mu V$
MHE	$0.019s$	0.36%	$126\mu V$

Table 4.7: Comparison of algorithm execution time and RMS error for various estimation algorithms in closed loop configuration for $3C$ charging current at 318K temperature. The simulated plant output voltage is considered a reference.

Algorithm	Algorithm execution time per iteration
SMO estimation based on SFHM model	$0.32ms$
SMO estimation based on SP2D model	$0.54ms$

Table 4.8: Comparison of algorithm execution time for sliding mode observer (SMO) based on simplified FHM model and simplified P2D model for $3C$ input current.

4.3 Results and discussion

The sample time for simulation is one second, the same as the sample time of the experiment. The experimental results are obtained from Harikesh's article [6]. The prediction and control horizon is three. The estimator's performance improves if the prediction and control horizon increase; however, the computational cost increases proportionally. So the minimum value of prediction and control horizon is sued, which gives satisfactory performance. The performance of EKF, SMO and MHE is compared with the experimental voltage obtained from [6]. An input current of $1C$ is applied, the variance of measurement noise and process noise is 1mV, and the mean is zero. The results are shown in figure 4.1, 4.2 and 4.3, respectively. The root mean square error (RMSE) of voltage output for EKF, SMO and MHE are 0.8%, 0.59% and 0.06%, respectively. Considering RMS error as a figure of merit, MHE shows superior performance, followed by SMO. However, SMO has minimum error variance. Algorithm execution time per iteration for whole code, i.e. estimator and plant for EKF, SMO and MHE, are 0.3ms, 0.2ms and 7ms, respectively. Algorithm execution time is calculated using Matlab *tic*, and *toc* commands for all simulations. The algorithm execution time for the estimation part of the code is 0.27ms, 0.17ms and 0.67ms for EKF, SMO and MHE, respectively. The difference between algorithm execution time for complete code and the estimation part of code is the same for all algorithms, i.e. 0.03ms, which implies only the estimation part of the code is different, and the comparison is genuine. Real-time implementation of the algorithms mentioned above is feasible as computation time is less than sample time. Fmincon is not a real-time estimator, i.e. the algorithm is not optimised for minimum execution time on computing hardware. It is used to illustrate the concept only. If the algorithm execution time for Fmincon for a single iteration is less than the sampling time, it is reasonable to assume that real-time NLP solvers will be faster than Fmincon. RMS error is calculated as follows.

$$RMS\ Error = \frac{100}{mean(V_{ref})} \times \sqrt{\frac{1}{N}\sum_{i=0}^{N}(V_{ref,i} - V_i)^2} \tag{4.25}$$

The effect of the perturbation on the estimator's performance is also studied. Simulated plant voltage is considered a reference. A sensor measures the output voltage of Li-ion. Noise is added to plant output voltage to model sensor noise, as mentioned in the following.

$$V_{measured} = V_{actual} + v_n \tag{4.26}$$

v_n is additive white Gaussian noise. V_{actual} is the actual voltage as given by output voltage equation 2.43. The mean noise value is zero volts, and the variance of the noise is one mV. In the rest of the article, the subscript *measured* is dropped as it is well-known that the output voltage is measured using the sensor. Noise is added to Li-ion cell states to model process noise, as mentioned in the following.

$$x_{actual} = x_{model} + w_n \tag{4.27}$$

w_n is additive white Gaussian noise. x_{model} is the Li-ion concentration predicted by the diffusion equation 2.18. The mean noise value is zero $1molm^{-3}$, and the variance of the noise is $1molm^{-3}$. Zero mean and unity variance noise can be generated using MATLAB *randn* command. A noise signal of desired mean and variance can be generated from the zero mean and unity variance signal. Let's assume w_{zn} is zero mean and unity variance signal. A noise signal w_n with required mean M_n and variance v_r can be generated by using the following equation.

$$w_n = w_{zn}(\sqrt{v_r}) + M_n \tag{4.28}$$

The results are shown in figures 4.4, 4.5 and 4.6, respectively. RMS error of voltage output for EKF, SMO and MHE are 0.03%, 0.04% and 0.04%, respectively. RMS error for the three estimators is similar. However, the error variance is minimum for SMO. Next, the diffusion equation is perturbed by 1%. Perturbation is achieved by changing the reciprocal of the length of the electrode and solid volume fraction by 1%. The results are shown in figure 4.7, 4.8 and 4.9, respectively. RMS error of voltage output for EKF, SMO and MHE are 0.2%, 0.05% and 0.05%, respectively. As EKF is based on the

concept of linearisation, perturbation deteriorates its performance to a greater extent as compared to others. The error variance is minimum for MHE as compared to SMO and EKF. It is observed that the performance of SMO degrades as perturbation increases to 3%. For example, the RMS error for 2% perturbation for SMO is 0.9%, whereas MHE performance remains unchanged. The performance of all estimators degrades when the perturbation is introduced in all parameters of the Li-ion cell. For example, the RMS error for MHE, SMO and EKF are 0.09%, 0.15% and 0.35% respectively for 1% perturbation in all parameters. Error variance is increased for SMO and EKF, whereas it remains unchanged for MHE.

The computation time per iteration for the SMO estimation based on the simplified FHM model and P2D model is $0.32ms$ and $0.54ms$, respectively, as shown in Table 4.8 reaffirming the computational efficiency of the simplified FHM model. The details of the simplified P2D model are given in [87].

Closed-loop control using MPC and the estimation algorithms are simulated. The output voltage and estimation error plots for MHE are shown in figure 4.10. Figure 4.11 shows estimation error for EKF and SMO. The estimation algorithms show performance similar to open-loop simulation results. Algorithm execution time and RMS error increase as the MPC charging algorithm is included in the loop. The Algorithm execution time per iteration for EKF, SMO and MHE are 7ms, 12.5ms and 30ms, respectively. The RMS errors of estimated output voltage for EKF, SMO and MHE are 3%, 3.6% and 0.36%, respectively. RMS error is the minimum for MHE. However, the error variance is quite high. Simulated plant voltage is considered a reference for calculating RMS error. The data suggests that real-time output feedback control is feasible using EKF, SMO and MHE in a loop. The sensor noise variance for closed-loop simulation is $0.2mV$, and the input current constraint is $3C$. The data is summarised in the table 4.7.

Chapter 5

Conclusion and future recommendations

5.1 Conclusion

A simplified FHM model is proposed and compared with a simplified P2D model in this study. The simplified FHM model is developed by approximating the diffusion equations. The basic idea of approximation is that polynomial functions can accurately estimate the Li-ion concentration. Approximation of intercalation current and conduction equations leads to the development of variants of the simplified FHM model to trade-off accuracy with computational cost. Simulation results verify its superior performance compared to the simplified P2D model. The computational time of the proposed model is 35% less than the FHM model and close to the simplified P2D model. The simplified FHM model has a tracking RMS error of 0.6%, while the simplified P2D model has a 2% tracking error. The model works accurately up to a current of $4C$ with a maximum 2.1% error. Health-conscious control of a Li-ion cell using the novel simplified FHM model is also discussed. Pseudo-spectral transcription or discretization using Chebyshev polynomials is utilised for converting the optimal control problem (OCP) into a nonlinear programming problem (NLP). The NLP is solved using nonlinear model predictive control (NMPC). MATLAB ® facility fmincon is used to implement the NMPC.

The performance of the charging algorithm is compared with the industry-standard

CCCV charging algorithm. We have observed that the health-conscious algorithm significantly reduces health degradation compared to the *CCCV* algorithm. The film resistance R_{film} and state of health (SoH) show less degradation when charged by the health-conscious controller as compared to the *CCCV* charging algorithm. SoH is defined based on the capacity degradation of a Li-ion cell.

The performance of both algorithms is analysed for a range of input current upper bound values. The algorithms show inferior performance at low values of input current upper bound, and the performance improves and stabilises at higher values.

Multiple cycle charging shows that the battery reaches the end of life (80% SoH) after 484 cycles for health-conscious and 392 cycles for *CCCV* charging. Charging a Li-ion cell with the health-conscious algorithm increases battery life by 92 cycles and reduces film resistance.

Output feedback control of a simplified FHM model of a Li-ion cell is implemented using an MPC and three estimation algorithms, i.e. EKF, SMO and MHE. The performance of output feedback control closely matches state feedback control which means that the observers accurately estimates the plant dynamics. Open-loop estimation comparison of the estimators reveals that MHE performs better than EKF and SMO when the output voltage signal is corrupted by additive white Gaussian noise. Another point we observed is that MHE maintains its performance when parameters are perturbed, whereas the performance of SMO and EKF degrades due to parameter perturbation. However, the simulation time per iteration is high for the MHE. Still, the computation time for the MHE is suitable for real-time implementation.

5.2 Future recommendations

Many variants of simplified models are presented in this work to trade-off accuracy and computational burden; however, we can develop more variants. For example, developing a linear model is a good step towards further simplification and reducing the computational load. We can apply either the transfer function or the state space approach.

The model discussed in the paper is isothermal. Temperature dynamics has a significant impact on mathematical model's performance. Incorporating the thermal dynamics of a cell will improve the accuracy of the simplified FHM model.

Li-ion cell charging is accomplished using only one control algorithm, i.e. an MPC. Comparison with algorithms such as reinforced learning control and classical control algorithms will provide further insight and enable us to compare the strengths and weaknesses of controllers.

Three estimation algorithms are studied to estimate SoC for improved performance in the presence of noise and parameter uncertainties. We recommend using other estimation algorithms to compare and analyse their strengths and weaknesses.

We have discussed modelling, charging and estimation for a single cell. This work can be extended to develop a model, charging and estimation algorithm for battery pack in the future.

Bibliography

[1] Adrien Bizeray. *State and parameter estimation of physics-based lithium-ion battery models*. PhD thesis, University of Oxford, 2016. 9, 17

[2] Zhongwei Deng, Lin Yang, Hao Deng, Yishan Cai, and Dongdong Li. Polynomial approximation pseudo-two-dimensional battery model for online application in embedded battery management system. *Energy*, 142:838–850, 2018. 9, 12, 18, 20, 27, 28, 39, 41

[3] Mehdi M Forouzan, Brian A Mazzeo, and Dean R Wheeler. Modeling the effects of electrode microstructural heterogeneities on li-ion battery performance and lifetime. *Journal of The Electrochemical Society*, 165(10):A2127, 2018. 9, 33

[4] Fangming Jiang and Peng Peng. Elucidating the performance limitations of lithium-ion batteries due to species and charge transport through five characteristic parameters. *Scientific reports*, 6(1):1–18, 2016. 9, 33, 34

[5] Mohammad Kamrul Hasan, Md Mahmud, AKM Ahasan Habib, SMA Motakabber, and Shayla Islam. Review of electric vehicle energy storage and management system: Standards, issues, and challenges. *Journal of Energy Storage*, 41:102940, 2021. 9, 12, 15, 34, 35, 37, 38, 39

[6] Harikesh Arunachalam and Simona Onori. Full homogenized macroscale model and pseudo-2-dimensional model for lithium-ion battery dynamics: Comparative analysis, experimental verification and sensitivity analysis. *Journal of The Electrochemical Society*, 166(8):A1380–A1392, 2019. 9, 10, 19, 22, 45, 48, 49, 50, 81, 82, 88

[7] Harikesh Arunachalam and Simona Onori. What if the doyle-fuller-newman model fails? a new macroscale modeling framework. In *2018 IEEE Conference on Decision and Control (CDC)*, pages 5702–5707. IEEE, 2018. 12, 19, 22, 29, 32, 45

[8] Rui Xiong, Jiayi Cao, Quanqing Yu, Hongwen He, and Fengchun Sun. Critical review on the battery state of charge estimation methods for electric vehicles. *Ieee Access*, 6:1832–1843, 2017. 12, 15, 34, 35

[9] Marc Doyle and John Newman. The use of mathematical modeling in the design of lithium/polymer battery systems. *Electrochimica Acta*, 40(13-14):2191–2196, 1995. 12, 34, 35

[10] Xuebing Han, Minggao Ouyang, Languang Lu, and Jianqiu Li. Simplification of physics-based electrochemical model for lithium ion battery on electric vehicle. part ii: Pseudo-two-dimensional model simplification and state of charge estimation. *Journal of Power Sources*, 278:814–825, 2015. 12, 18, 20, 27, 39, 41

[11] Eduardo F Camacho and Carlos Bordons. Nonlinear model predictive control. In *Model Predictive control*, pages 249–288. Springer, 2007. 12, 61, 74, 76, 80

[12] Gregory L Plett. Extended kalman filtering for battery management systems of lipb-based hev battery packs: Part 2. modeling and identification. *Journal of power sources*, 134(2):262–276, 2004. 14, 16, 71

[13] Gregory L Plett. Extended kalman filtering for battery management systems of lipb-based hev battery packs: Part 3. state and parameter estimation. *Journal of Power sources*, 134(2):277–292, 2004. 14, 16, 71

[14] Kailong Liu, Kang Li, Qiao Peng, and Cheng Zhang. A brief review on key technologies in the battery management system of electric vehicles. *Frontiers of Mechanical Engineering*, 14(1):47–64, 2019. 15

[15] Jinhao Meng, Mattia Ricco, Guangzhao Luo, Maciej Swierczynski, Daniel-Ioan Stroe, Ana-Irina Stroe, and Remus Teodorescu. An overview and comparison

of online implementable soc estimation methods for lithium-ion battery. *IEEE Transactions on Industry Applications*, 54(2):1583–1591, 2017. 15

[16] Wenlu Zhou, Yanping Zheng, Zhengjun Pan, and Qiang Lu. Review on the battery model and soc estimation method. *Processes*, 9(9):1685, 2021. 15, 23, 68

[17] Xiaosong Hu, Shengbo Li, and Huei Peng. A comparative study of equivalent circuit models for li-ion batteries. *Journal of Power Sources*, 198:359–367, 2012. 16, 27

[18] Jinhao Meng, Guangzhao Luo, Mattia Ricco, Maciej Swierczynski, Daniel-Ioan Stroe, and Remus Teodorescu. Overview of lithium-ion battery modeling methods for state-of-charge estimation in electrical vehicles. *Applied sciences*, 8(5):659, 2018. 16

[19] Xiaoqiang Zhang, Weiping Zhang, and Geyang Lei. A review of li-ion battery equivalent circuit models. *Transactions on Electrical and Electronic Materials*, 17(6):311–316, 2016. 16

[20] Shunli Wang, Carlos Fernandez, Chunmei Yu, Yongcun Fan, Wen Cao, and Daniel-Ioan Stroe. A novel charged state prediction method of the lithium ion battery packs based on the composite equivalent modeling and improved splice kalman filtering algorithm. *Journal of power sources*, 471:228450, 2020. 17

[21] Mohamed A Awadallah and Bala Venkatesh. Accuracy improvement of soc estimation in lithium-ion batteries. *Journal of Energy Storage*, 6:95–104, 2016. 17

[22] Krishna Veer Singh, Hari Om Bansal, and Dheerendra Singh. Hardware-in-the-loop implementation of anfis based adaptive soc estimation of lithium-ion battery for hybrid vehicle applications. *Journal of Energy Storage*, 27:101124, 2020. 17

[23] Chaofan Yang, Xueyuan Wang, Qiaohua Fang, Haifeng Dai, Yaqian Cao, and Xuezhe Wei. An online soc and capacity estimation method for aged lithium-ion

battery pack considering cell inconsistency. *Journal of Energy Storage*, 29:101250, 2020. 17

[24] L Ma, C Hu, and F Cheng. State of charge and state of energy estimation for lithium-ion batteries based on a long short-term memory neural network. *Journal of Energy Storage*, 37:102440, 2021. 17

[25] Hao Yang, Xianzhong Sun, Yabin An, Xiong Zhang, Tongzhen Wei, and Yanwei Ma. Online parameters identification and state of charge estimation for lithium-ion capacitor based on improved cubature kalman filter. *Journal of Energy Storage*, 24:100810, 2019. 17

[26] Hafiz Farhaj Khan, Aamir Hanif, Muhammad Umair Ali, and Amad Zafar. A lagrange multiplier and sigma point kalman filter based fused methodology for online state of charge estimation of lithium-ion batteries. *Journal of Energy Storage*, 41:102843, 2021. 17, 71

[27] Marc Doyle and John Newman. The use of mathematical modeling in the design of lithium/polymer battery systems. *Electrochimica Acta*, 40(13-14):2191–2196, 1995. 17

[28] Liuying Li, Yaxing Ren, Kieran O'Regan, Upender Rao Koleti, Emma Kendrick, W Dhammika Widanage, and James Marco. Lithium-ion battery cathode and anode potential observer based on reduced-order electrochemical single particle model. *Journal of Energy Storage*, 44:103324, 2021. 18

[29] Lichao Ren, Guorong Zhu, Jianqiang Kang, Jing V Wang, Bingyang Luo, Chaoyang Chen, and Kui Xiang. An algorithm for state of charge estimation based on a single-particle model. *Journal of Energy Storage*, 39:102644, 2021. 18

[30] Tanvir R Tanim, Christopher D Rahn, and Chao-Yang Wang. State of charge estimation of a lithium ion cell based on a temperature dependent and electrolyte enhanced single particle model. *Energy*, 80:731–739, 2015. 18, 27

[31] Meng Guo, Godfrey Sikha, and Ralph E White. Single-particle model for a lithium-ion cell: Thermal behavior. *Journal of The Electrochemical Society*, 158(2):A122, 2010. 18

[32] Rohit Mehta and Amit Gupta. An improved single-particle model with electrolyte dynamics for high current applications of lithium-ion cells. *Electrochimica Acta*, 389:138623, 2021. 18

[33] Venkat R Subramanian, Vinten D Diwakar, and Deepak Tapriyal. Efficient macro-micro scale coupled modeling of batteries. *Journal of The Electrochemical Society*, 152(10):A2002–A2008, 2005. 18, 20, 28, 35

[34] Tanvir R Tanim, Christopher D Rahn, and Chao-Yang Wang. State of charge estimation of a lithium ion cell based on a temperature dependent and electrolyte enhanced single particle model. *Energy*, 80:731–739, 2015. 18, 31

[35] Karthikeyan Kumaresan, Godfrey Sikha, and Ralph E White. Thermal model for a li-ion cell. *Journal of the Electrochemical Society*, 155(2):A164, 2007. 18

[36] Seyed Saeed Madani, Erik Schaltz, and Søren Knudsen Kær. Review of parameter determination for thermal modeling of lithium ion batteries. *Batteries*, 4(2):20, 2018. 18

[37] Kandler A Smith, Christopher D Rahn, and Chao-Yang Wang. Control oriented 1d electrochemical model of lithium ion battery. *Energy Conversion and management*, 48(9):2565–2578, 2007. 18

[38] James L Lee, Andrew Chemistruck, and Gregory L Plett. One-dimensional physics-based reduced-order model of lithium-ion dynamics. *Journal of Power Sources*, 220:430–448, 2012. 18

[39] Ngoc Tham Tran, Mahinda Vilathgamuwa, Troy Farrell, Yang Li, Joseph Teague, et al. A padé approximate model of lithium ion batteries. *Journal of The Electrochemical Society*, 165(7):A1409, 2018. 18

[40] James L Lee, Andrew Chemistruck, and Gregory L Plett. Discrete-time realization of transcendental impedance models, with application to modeling spherical solid diffusion. *Journal of Power Sources*, 206:367–377, 2012. 19

[41] Harikesh Arunachalam, Svyatoslav Korneev, Ilenia Battiato, and Simona Onori. Multiscale modeling approach to determine effective lithium-ion transport properties. In *2017 American Control Conference (ACC)*, pages 92–97. IEEE, 2017. 19, 45

[42] Nalin A Chaturvedi, Reinhardt Klein, Jake Christensen, Jasim Ahmed, and Aleksandar Kojic. Algorithms for advanced battery-management systems. *IEEE Control systems magazine*, 30(3):49–68, 2010. 19, 28, 42, 55

[43] Fernando A Ortiz-Ricardez, Aldo Romero-Becerril, and Luis Alvarez-Icaza. Hard limitations of polynomial approximations for reduced-order models of lithium-ion cells. *Journal of Applied Electrochemistry*, 50(3):343–354, 2020. 20, 28

[44] Qian Lin, Jun Wang, Rui Xiong, Weixiang Shen, and Hongwen He. Towards a smarter battery management system: A critical review on optimal charging methods of lithium ion batteries. *Energy*, 183:220–234, 2019. 20

[45] Yizhao Gao, Xi Zhang, Qiyu Cheng, Bangjun Guo, and Jun Yang. Classification and review of the charging strategies for commercial lithium-ion batteries. *IEEE Access*, 7:43511–43524, 2019. 20

[46] Wenlong Xie, Xinhua Liu, Rong He, Yalun Li, Xinlei Gao, Xinghu Li, Zhaoxia Peng, Suwei Feng, Xuning Feng, and Shichun Yang. Challenges and opportunities toward fast-charging of lithium-ion batteries. *Journal of Energy Storage*, 32:101837, 2020. 20

[47] Sheng Shui Zhang. The effect of the charging protocol on the cycle life of a li-ion battery. *Journal of power sources*, 161(2):1385–1391, 2006. 20

[48] Muhammad Nizam, Hari Maghfiroh, Bayhaqi Irfani, Inayati Inayati, and Alfian

Ma'arif. Designing and prototyping of lithium-ion charging system using multi-step constant current method. *World Electric Vehicle Journal*, 13(10):178, 2022. 21

[49] Guan-Jhu Chen, Yi-Hua Liu, Shun-Chung Wang, Yi-Feng Luo, and Zong-Zhen Yang. Searching for the optimal current pattern based on grey wolf optimizer and equivalent circuit model of li-ion batteries. *Journal of Energy Storage*, 33:101933, 2021. 21

[50] Anna Tomaszewska, Zhengyu Chu, Xuning Feng, Simon O'kane, Xinhua Liu, Jingyi Chen, Chenzhen Ji, Elizabeth Endler, Ruihe Li, Lishuo Liu, et al. Lithium-ion battery fast charging: A review. *ETransportation*, 1:100011, 2019. 21

[51] Qian Lin, Jun Wang, Rui Xiong, Weixiang Shen, and Hongwen He. Towards a smarter battery management system: A critical review on optimal charging methods of lithium ion batteries. *Energy*, 183:220–234, 2019. 21

[52] Ji Liu, Guang Li, and Hosam K Fathy. An extended differential flatness approach for the health-conscious nonlinear model predictive control of lithium-ion batteries. *IEEE Transactions on Control Systems Technology*, 25(5):1882–1889, 2016. 21, 53, 58

[53] MSS Malik, Guang Li, and Zheng Chen. An optimal charging algorithm to minimise solid electrolyte interface layer in lithium-ion battery. *Journal of Power Sources*, 482:228895, 2021. 21, 53, 58

[54] Xiaosong Hu, Yusheng Zheng, Xianke Lin, and Yi Xie. Optimal multistage charging of nca/graphite lithium-ion batteries based on electrothermal-aging dynamics. *IEEE Transactions on Transportation Electrification*, 6(2):427–438, 2020. 21, 53

[55] Hector Eduardo Perez, Xiaosong Hu, Satadru Dey, and Scott J. Moura. Optimal charging of li-ion batteries with coupled electro-thermal-aging dynamics. *IEEE Transactions on Vehicular Technology*, 66(9):7761–7770, 2017. 21

[56] P Ramadass, Bala Haran, Parthasarathy M Gomadam, Ralph White, and Branko N

Popov. Development of first principles capacity fade model for li-ion cells. *Journal of the Electrochemical Society*, 151(2):A196, 2004. 21, 22, 24, 53, 54, 70

[57] M Safari, Mathieu Morcrette, A Teyssot, and Charles Delacourt. Multimodal physics-based aging model for life prediction of li-ion batteries. *Journal of The Electrochemical Society*, 156(3):A145, 2008. 21, 22, 24, 53, 54, 70

[58] Andrew Carnovale and Xianguo Li. A modeling and experimental study of capacity fade for lithium-ion batteries. *Energy and AI*, 2:100032, 2020. 21

[59] Anirudh Allam and Simona Onori. Online capacity estimation for lithium-ion battery cells via an electrochemical model-based adaptive interconnected observer. *IEEE Transactions on Control Systems Technology*, 29(4):1636–1651, 2020. 21

[60] Zuan Khalik, Henk Jan Bergveld, and MCF Donkers. Ageing-aware charging of lithium-ion batteries using an electrochemistry-based model with capacity-loss side reactions. In *2020 American Control Conference (ACC)*, pages 2213–2218. IEEE, 2020. 21, 64

[61] Andrea Pozzi, Marcello Torchio, and Davide M Raimondo. Film growth minimization in a li-ion cell: a pseudo two dimensional model-based optimal charging approach. In *2018 European Control Conference (ECC)*, pages 1753–1758. IEEE, 2018. 21

[62] Shichun Yang, Xinlei Gao, Yalun Li, Wenlong Xie, Bin Guo, Lisheng Zhang, and Xinhua Liu. Minimum lithium plating overpotential control based charging strategy for parallel battery module prevents side reactions. *Journal of Power Sources*, 494:229772, 2021. 21, 53

[63] Yilin Yin, Yalan Bi, Yang Hu, and Song-Yul Choe. Optimal fast charging method for a large-format lithium-ion battery based on nonlinear model predictive control and reduced order electrochemical model. *Journal of the Electrochemical Society*, 167(16):160559, 2021. 22, 24, 53, 70

[64] Jiangtao He, Shujuan Meng, and Fengjun Yan. A comparative study of soc

estimation based on equivalent circuit models. *Frontiers in Energy Research*, page 676, 2022. 23

[65] Mohammad A Hannan, MS Hossain Lipu, Aini Hussain, and Azah Mohamed. A review of lithium-ion battery state of charge estimation and management system in electric vehicle applications: Challenges and recommendations. *Renewable and Sustainable Energy Reviews*, 78:834–854, 2017. 23, 68

[66] Bharatkumar Suthar, Venkatasailanathan Ramadesigan, Paul WC Northrop, Bhushan Gopaluni, Shriram Santhanagopalan, Richard D Braatz, and Venkat R Subramanian. Optimal control and state estimation of lithium-ion batteries using reformulated models. In *2013 American Control Conference*, pages 5350–5355. IEEE, 2013. 23, 24, 69

[67] Jiani Shen, Qiankun Wang, Guangjin Zhao, Zifeng Ma, and Yijun He. A joint moving horizon strategy for state-of-charge estimation of lithium-ion batteries under combined measurement uncertainty. *Journal of Energy Storage*, 44:103316, 2021. 23, 69

[68] Bruno Morabito, Reinhardt Klein, and Rolf Findeisen. Real time feasibility and performance of moving horizon estimation for li-ion batteries based on first principles electrochemical models. In *2017 American Control Conference (ACC)*, pages 3457–3462. IEEE, 2017. 23, 69

[69] Jian Hu, Zhongbao Wei, and Hongwen He. Moving horizon estimation based unknown input observer for lithium-ion batteries. In *2021 IEEE 12th Energy Conversion Congress & Exposition-Asia (ECCE-Asia)*, pages 959–962. IEEE, 2021. 23, 69

[70] Ji Liu, Sergio Mendoza, and Hosam K Fathy. Total least squares state of charge estimation for lithium-ion batteries: An efficient moving horizon estimation approach. *IFAC-PapersOnLine*, 50(1):14489–14494, 2017. 23, 69

[71] Hongbin Ren, Hongwei Zhang, Zepeng Gao, et al. A robust approach to state of charge assessment based on moving horizon optimal estimation considering

battery system uncertainty and aging condition. *Journal of Cleaner Production*, 270:122508, 2020. 23, 69

[72] Ma Yan, Zhou Xiuwen, and Zhang Jixing. Lithium-ion battery state of charge estimation based on moving horizon. In *Proceeding of the 11th World Congress on Intelligent Control and Automation*, pages 5002–5007. IEEE, 2014. 23, 69

[73] Xiaosong Hu, Dongpu Cao, and Bo Egardt. Condition monitoring in advanced battery management systems: Moving horizon estimation using a reduced electrochemical model. *IEEE/ASME Transactions on Mechatronics*, 23(1):167–178, 2017. 23, 69

[74] Jia-Ni Shen, Yi-Jun He, Zi-Feng Ma, Hong-Bin Luo, and Zi-Feng Zhang. Online state of charge estimation of lithium-ion batteries: A moving horizon estimation approach. *Chemical Engineering Science*, 154:42–53, 2016. 23, 69

[75] Jia-Ni Shen, Jia-Jin Shen, Yi-Jun He, and Zi-Feng Ma. Accurate state of charge estimation with model mismatch for li-ion batteries: a joint moving horizon estimation approach. *IEEE Transactions on Power Electronics*, 34(5):4329–4342, 2018. 23, 69

[76] Yong Chen, Changlong Li, Sizhong Chen, Hongbin Ren, and Zepeng Gao. A combined robust approach based on auto-regressive long short-term memory network and moving horizon estimation for state-of-charge estimation of lithium-ion batteries. *International Journal of Energy Research*, 45(9):12838–12853, 2021. 23, 69

[77] Abbas Fotouhi, Daniel J Auger, Karsten Propp, Stefano Longo, and Mark Wild. A review on electric vehicle battery modelling: From lithium-ion toward lithium–sulphur. *Renewable and Sustainable Energy Reviews*, 56:1008–1021, 2016. 27

[78] Steven K Kauwe, Trevor David Rhone, and Taylor D Sparks. Data-driven studies of li-ion-battery materials. *Crystals*, 9(1):54, 2019. 27

[79] Juan Pablo Rivera-Barrera, Nicolás Muñoz-Galeano, and Henry Omar Sarmiento-Maldonado. Soc estimation for lithium-ion batteries: Review and future challenges. *Electronics*, 6(4):102, 2017. 27

[80] Scott J Moura, Federico Bribiesca Argomedo, Reinhardt Klein, Anahita Mirtabatabaei, and Miroslav Krstic. Battery state estimation for a single particle model with electrolyte dynamics. *IEEE Transactions on Control Systems Technology*, 25(2):453–468, 2016. 27, 42

[81] Venkat R Subramanian, Vinten D Diwakar, and Deepak Tapriyal. Efficient macro-micro scale coupled modeling of batteries. *Journal of The Electrochemical Society*, 152(10):A2002–A2008, 2005. 27

[82] Lars Ole Valøen and Jan N Reimers. Transport properties of lipf6-based li-ion battery electrolytes. *Journal of The Electrochemical Society*, 152(5):A882–A891, 2005. 28, 43

[83] Morris Brenna, Federica Foiadelli, Carola Leone, and Michela Longo. Electric vehicles charging technology review and optimal size estimation. *Journal of Electrical Engineering & Technology*, 15(6):2539–2552, 2020. 52

[84] Jinlei Sun, Qian Ma, Ruihang Liu, Tianru Wang, and Chuanyu Tang. A novel multiobjective charging optimization method of power lithium-ion batteries based on charging time and temperature rise. *International Journal of Energy Research*, 43(13):7672–7681, 2019. 53

[85] Robin Drees, Frank Lienesch, and Michael Kurrat. Fast charging lithium-ion battery formation based on simulations with an electrode equivalent circuit model. *Journal of Energy Storage*, 36:102345, 2021. 53

[86] Reinhardt Klein, Nalin A Chaturvedi, Jake Christensen, Jasim Ahmed, Rolf Findeisen, and Aleksandar Kojic. Optimal charging strategies in lithium-ion battery. In *Proceedings of the 2011 american Control Conference*, pages 382–387. IEEE, 2011. 53

[87] Salman Qadir, Guang Li, and Zheng Chen. Simplification of full homogenized macro-scale model for lithium-ion batteries. *Journal of Energy Storage*, 46:103801, 2022. 54, 63, 69, 90

[88] Lloyd N Trefethen. Spectral methods in matlab, volume 10 of software, environments, and tools. *Society for Industrial and Applied Mathematics (SIAM), Philadelphia, PA*, 24, 2000. 57

[89] J Andre Weideman and Satish C Reddy. A matlab differentiation matrix suite. *ACM Transactions on Mathematical Software (TOMS)*, 26(4):465–519, 2000. 57

[90] MSS Malik, Guang Li, and Zheng Chen. An optimal charging algorithm to minimise solid electrolyte interface layer in lithium-ion battery. *Journal of Power Sources*, 482:228895, 2021. 64

[91] Changfu Zou, Chris Manzie, and Dragan Nešić. Model predictive control for lithium-ion battery optimal charging. *IEEE/ASME Transactions on Mechatronics*, 23(2):947–957, 2018. 69

[92] Changfu Zou, Xiaosong Hu, Zhongbao Wei, Torsten Wik, and Bo Egardt. Electrochemical estimation and control for lithium-ion battery health-aware fast charging. *IEEE Transactions on Industrial Electronics*, 65(8):6635–6645, 2017. 69

[93] Anirudh Allam and Simona Onori. Linearized versus nonlinear observability analysis for lithium-ion battery dynamics: Why respecting the nonlinearities is key for proper observer design. *IEEE Access*, 9:163431–163440, 2021. 70

[94] Domenico Di Domenico, Anna Stefanopoulou, and Giovanni Fiengo. Lithium-Ion Battery State of Charge and Critical Surface Charge Estimation Using an Electrochemical Model-Based Extended Kalman Filter. *Journal of Dynamic Systems, Measurement, and Control*, 132(6), October 2010. 70

[95] Dong Zhang, Satadru Dey, Luis D. Couto, and Scott J. Moura. Battery Adaptive Observer for a Single-Particle Model With Intercalation-Induced Stress. *IEEE*

Transactions on Control Systems Technology, 28(4):1363–1377, July 2020. Conference Name: IEEE Transactions on Control Systems Technology. 70

[96] Stefano Marelli and Matteo Corno. A mass-preserving sliding mode observer for li-ion cells electrochemical model. In *2018 European Control Conference (ECC)*, pages 2659–2664. IEEE, 2018. 70, 73

[97] Scott J Moura, Nalin A Chaturvedi, and Miroslav Krstić. Adaptive partial differential equation observer for battery state-of-charge/state-of-health estimation via an electrochemical model. *Journal of Dynamic Systems, Measurement, and Control*, 136(1):011015, 2014. 71

[98] Ngoc Tham Tran, Mahinda Vilathgamuwa, Yang Li, Troy Farrell, Joseph Teague, et al. State of charge estimation of lithium ion batteries using an extended single particle model and sigma-point kalman filter. In *2017 IEEE Southern Power Electronics Conference (SPEC)*, pages 1–6. IEEE, 2017. 71

[99] Oliver Olson. A comparative study of the extended kalman filter and sliding mode observer for orbital determination for formation flying about the l (2) lagrange point. Master's thesis, University of New Hampshire, 2007. 73

[100] Xin Sui, Shan He, Daniel-Ioan Stroe, Xinrong Huang, Jinhao Meng, and Remus Teodorescu. A review of sliding mode observers based on equivalent circuit model for battery soc estimation. In *2019 IEEE 28th International Symposium on Industrial Electronics (ISIE)*, pages 1965–1970. IEEE, 2019. 73

[101] Warren E Stewart and Jan P Sorensen. New algorithms for nonlinear least squares and bayesian parameter estimation. Technical report, WISCONSIN UNIV-MADISON MATHEMATICS RESEARCH CENTER, 1980. 76

[102] Christopher V Rao. *Moving horizon strategies for the constrained monitoring and control of nonlinear discrete-time systems*. The University of Wisconsin-Madison, 2000. 77